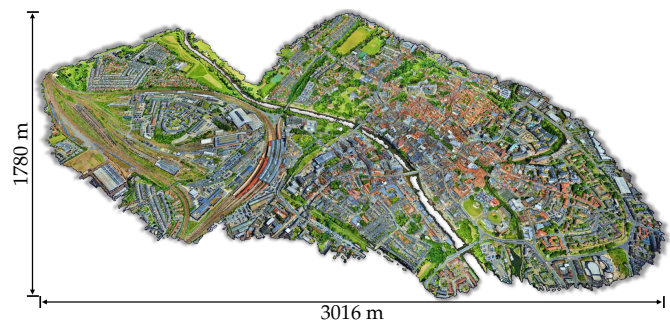


# SensatUrban: Learning Semantics from Urban-Scale Photogrammetric Point Clouds

Qingyong Hu · Bo Yang · Sheikh Khalid · Wen Xiao · Niki Trigoni · Andrew Markham

Received: date / Accepted: date

**Abstract** With the recent availability and affordability of commercial depth sensors and 3D scanners, an increasing number of 3D (*i.e.*, RGBD, point cloud) datasets have been publicized to facilitate research in 3D computer vision. However, existing datasets either cover relatively small areas or have limited semantic annotations. Fine-grained understanding of urban-scale 3D scenes is still in its infancy. In this paper, we introduce SensatUrban, an urban-scale UAV photogrammetry point cloud dataset consisting of nearly three billion points collected from three UK cities, covering 7.6  $km^2$ . Each point in the dataset has been labelled with fine-grained semantic annotations, resulting in a dataset that is three times the size of the previous existing largest photogrammetric point cloud dataset. In addition to the more commonly encountered categories such as road and vegetation, urban-level categories including rail, bridge, and river are also included in our dataset. Based on this dataset, we further build a benchmark to evaluate the performance of state-of-the-art segmentation algorithms. In particular, we provide a comprehensive analysis and identify several key challenges limiting urban-scale point cloud understanding. The dataset



**Fig. 1** This shows an example of urban-scale point clouds in our SensatUrban dataset. It is acquired from the city center of York through UAV photogrammetry. It has a spatial coverage of more than 3 square kilometers and represents a typical urban suburb.

is available at <http://point-cloud-analysis.cs.ox.ac.uk/>.

**Keywords** Urban-Scale · Photogrammetric Point Cloud Dataset · Semantic Segmentation · UAV Photogrammetry

## 1 Introduction

Giving machines the ability to semantically interpret 3D scenes is highly important for accurate 3D perception and scene understanding. This is also the prerequisite for numerous real-world applications such as object-level robotic grasping [Rao et al. \(2010\)](#), scene-level robot navigation [Valada et al. \(2017\)](#) and autonomous driving [Geiger et al. \(2013\)](#), or even large-scale urban 3D modeling, where autonomous machines are required to interact competently within our physical world. Although increasing research attention has been applied to this field, it remains challenging due to the high geometrical complexity of urban scenes, and limited high quality labelled data resources.

Qingyong Hu · Niki Trigoni · Andrew Markham  
Department of Computer Science,  
University of Oxford  
E-mail: [firstname.lastname@cs.ox.ac.uk](mailto:firstname.lastname@cs.ox.ac.uk)

Bo Yang  
Department of Computing,  
The Hong Kong Polytechnic University,  
E-mail: [bo.yang@polyu.edu.hk](mailto:bo.yang@polyu.edu.hk)

Sheikh Khalid  
Sensat Ltd.

Wen Xiao  
School of Engineering,  
Newcastle University  
E-mail: [wen.xiao@newcastle.ac.uk](mailto:wen.xiao@newcastle.ac.uk)

Recently, an increasingly number of sophisticated neural pipelines have been proposed based on different representations of 3D scenes, including: 1) 3D voxel-based methods such as SegCloud [Tchapmi et al. \(2017\)](#), SparseConvNet [Graham et al. \(2018\)](#), MinkowskiNet [Choy et al. \(2019\)](#), PVCNN [Liu et al. \(2019\)](#), Cylinder3D [Zhu et al. \(2021\)](#) and 2) 2D projection-based approaches such as RangeNet++ [Milioto et al. \(2019\)](#), SalsaNext [Cortinhal et al. \(2020\)](#) and SqueezeSeg [Wu et al. \(2018a\)](#), PolarNet [Zhang et al. \(2020\)](#) and 3) recent point-based architectures *e.g.* PointNet/PointNet++ [Qi et al. \(2017a,b\)](#), PointCNN [Li et al. \(2018\)](#), DGCNN [Wang et al. \(2019b\)](#), KPConv [Thomas et al. \(2019\)](#), RandLA-Net [Hu et al. \(2020\)](#) and PointTransformer [Zhao et al. \(2020\)](#).

The core of these techniques, however, relies heavily on the wide availability of large-scale and high-quality open datasets. The datasets provide realistic and diverse data resources and act as benchmarks to fairly evaluate and compare the performance of different algorithms. Existing representative 3D data repositories can be generally classified as: 1) object-level 3D models such as ModelNet [Wu et al. \(2015\)](#), ShapeNet [Chang et al. \(2015\)](#) and ScanObjectNN [Uy et al. \(2019\)](#), 2) indoor scene-level 3D scans, *e.g.*, S3DIS [Armeni et al. \(2017\)](#), ScanNet [Dai et al. \(2017\)](#), Matterport3D [Chang et al. \(2018\)](#) and SceneNN [Zhou et al. \(2017\)](#), and 3) outdoor roadway-level 3D point clouds including Semantic3D [Hackel et al. \(2017\)](#), SemanticKITTI [Behley et al. \(2019\)](#), NPM3D [Roynard et al. \(2018\)](#), and Toronto3D [Tan et al. \(2020\)](#).

However, there is no large-scale photorealistic 3D point cloud dataset available for fine-grained semantic understanding of urban scenarios. Moreover, it remains an open question as to whether existing techniques can be scaled to these urban-scale point clouds. **Firstly**, in contrast to existing datasets for objects, rooms, or streets which are usually less than 200m in scale, the urban-scale datasets collected by aerial platforms typically span extremely wide areas, *e.g.* kilometres. How to efficiently and effectively preprocess massive point sets (*e.g.*, over  $10^8$ ) to feed into neural networks is a particular question of interest. **Secondly**, existing photogrammetric mapping techniques allow reconstructing photorealistic colored point clouds. Along with the 3D spatial coordinates, is the inclusion of appearance beneficial to semantic understanding and what is the impact if any? **Thirdly**, real-world urban scenarios usually exhibit extreme class imbalance. The majority of points are dominated by categories such as ground and vegetation, while the critical categories such as rail and water only occupy a small proportion of the total number of points. **Fourthly**, and potentially most importantly, what is the generalization performance of existing deep neural networks? Can a trained model be well-generalized to unseen data, particularly from a different region? or even generalized to different dataset? **Lastly**, is it possible to learn semantics with sparser labels? How can we unleash the potential of

self-supervised pre-training and semi-supervised learning on 3D point clouds?

In this paper, we take a step towards resolving the above issues. In particular, we first build a UAV photogrammetric point cloud dataset called **SensatUrban** for urban-scale 3D semantic understanding. This dataset covers  $7.6 \text{ km}^2$  of urban areas in three UK cities *i.e.*, Birmingham, Cambridge, and York (Figure 1), along with nearly 3 billion richly annotated 3D points. Each point in the Birmingham and Cambridge set is enriched with one of 13 predefined semantic categories such as *ground, vegetation, car, etc.*, while the points in York remain unlabeled for potential semi-supervised researches. The 3D point clouds are reconstructed from highly overlapped sequential aerial images captured by a professional-grade UAV mapping system. For more detailed data acquisition pipelines, please refer to Section 3. Compared with existing 3D datasets, the uniqueness of our SensatUrban lies in two aspects:

- **Urban-scale spatial coverage.** In contrast to existing datasets which mainly focus on objects [Wu et al. \(2015\)](#); [Chang et al. \(2015\)](#), rooms [Zhou et al. \(2017\)](#); [Armeni et al. \(2017\)](#); [Dai et al. \(2017\)](#) and roadways [Hackel et al. \(2017\)](#); [Behley et al. \(2019\)](#); [Roynard et al. \(2018\)](#); [Tan et al. \(2020\)](#), the point clouds in our SensatUrban dataset continuously cover several square kilometers of real-world urban areas, opening up new opportunities towards urban-scale applications such as smart cities, and national infrastructure planning and management.
- **Photorealistic and dense point clouds.** Our dataset is reconstructed from high-resolution aerial images captured by professional calibrated cameras. Unique aerial images from nadir (top-down) and oblique perspectives for the entire landscape of cities are also provided for optimized and high-quality point clouds. Naturally, the geometric patterns, textures, natural colors, point density, and distributions are distinct from existing LiDAR-based datasets.

Based on the proposed SensatUrban dataset, we further highlight several new challenges faced by generalizing existing segmentation algorithms to urban-scale point clouds in Section 5. In particular, these challenges include urban-scale data preparation, the usage of color information, learning from extremely imbalanced class distribution, cross-city generalization, and weakly and self-supervised learning from urban-scale point clouds. Note that, this paper does not aim to fully tackle these challenges, but to unveil them and provide insights to the community for future exploration.

To summarize, the main contributions of this paper are as follows:

- We propose a new urban-scale photogrammetric point cloud dataset for 3D semantic understanding, with an unprecedented spatial coverage at fine scale and rich semantic annotations.

- We provide a comprehensive benchmark for semantic segmentation of urban-scale point clouds. Extensive experimental results of different state-of-the-art approaches are provided, with detailed discussions and analysis.
- We highlight several unique challenges faced by generalizing existing neural pipelines to extremely large-scale point clouds, and provide an in-depth outlook of the future directions of 3D semantic learning.

A preliminary version of this work has been published in [Hu et al. \(2021\)](#), this journal extension particularly provides more details with regards to the data collection and point cloud reconstruction, additional experimental results and analysis in cross-dataset generalization, and weakly supervised semantic segmentation of urban-scale point clouds. In addition, the first challenge on large-scale point cloud analysis for urban scene understanding held in ICCV 2021 is based on this dataset. For more details, please refer to <https://urban3dchallenge.github.io/>.

## 2 Related Work

### 2.1 Datasets for 3D Scene Understanding

We first give a brief introduction to the dataset used for 3D scene understanding. For a comprehensive survey, please refer to [Guo et al. \(2020\)](#) for more details.

In general, existing representative datasets can be roughly categorized into the following four subgroups based on the spatial coverage: **1) Object-level 3D models.** Early datasets are mainly focused on the recognition of individual objects, thereby usually composed of a collection of synthetic 3D CAD models. Representative datasets include the synthetic ModelNet [Wu et al. \(2015\)](#), ShapeNet [Chang et al. \(2015\)](#), ShapePartNet [Yi et al. \(2016\)](#), PartNet [Mo et al. \(2019\)](#) and the real-world ScanObjectNN [Uy et al. \(2019\)](#). **2) Indoor scene-level 3D scans.** These datasets are usually acquired and further reconstructed by using commodity short-range depth scanners in indoor environments, including NYU3D [Silberman et al. \(2012\)](#), SUN RGB-D [Song et al. \(2015\)](#), S3DIS [Armeni et al. \(2017\)](#), SceneNN [Zhou et al. \(2017\)](#), Matterport3D [Chang et al. \(2018\)](#) and ScanNet [Dai et al. \(2017\)](#). Additionally, the SceneNet [Handa et al. \(2016\)](#) and SceneNet RGB-D [McCormac et al. \(2016\)](#) dataset also provide large-scale photorealistic rendering of indoor synthetic layouts. **3) Outdoor roadway-level 3D point clouds.** Most of these datasets are driven by the increasing demand of autonomous driving application, and usually collected by using modern laser scanner systems, including static Terrestrial Laser Scanners (TLS) and Mobile Laser Scanners (MLS). Representative datasets include the early Oakland [Munoz et al. \(2009\)](#), KITTI [Geiger et al. \(2012\)](#), Sydney Urban Objects [De Deuge et al. \(2013\)](#) and the recent Semantic3D

[Hackel et al. \(2017\)](#), Paris-Lille-3D [Roynard et al. \(2018\)](#), Argoverse [Chang et al. \(2019\)](#), SemanticKITTI [Behley et al. \(2019\)](#), SemanticPOSS [Pan et al. \(2020\)](#), Toronto-3D [Tan et al. \(2020\)](#), nuScenes [Caesar et al. \(2020\)](#), A2D2 [Geyer et al. \(2020\)](#), CSPC-Dataset [Tong et al. \(2020\)](#), Lyft dataset<sup>1</sup> and Waymo dataset [Sun et al. \(2020\)](#). Additionally, synthetic datasets [Ros et al. \(2016\)](#); [Gaidon et al. \(2016\)](#) composed of realistic simulation of LiDAR point clouds are also included. **4) Urban-level aerial 3D point clouds.** These datasets are usually acquired by professional-grade airborne LiDAR systems, including the recent DublinCity [Zolanvari et al. \(2019\)](#), DALES [Varney et al. \(2020\)](#) and LASDU [Ye et al. \(2020\)](#). Lacking the color information is the main limitation of these datasets, especially for the fine-grained semantic understanding of 3D scenarios. Interestingly, the very recent OpenGF [Qin et al. \(2021\)](#) dataset has started to investigate ultra-large-scale ground filtering datasets. However, this dataset mainly focuses on the task of ground extraction, instead of the fine-grained semantic understanding.

The recent Campus3D [Li et al. \(2020\)](#) 3DOM [Özdemir et al. \(2019\)](#), and H3D [Kölle et al. \(2021\)](#) are the most similar datasets to our SensatUrban datasets. They are also composed of large-scale photogrammetric 3D point clouds generated from high-resolution aerial images. However, our SensatUrban provides larger-scale 3D urban scenes with several times the number of points, as well as richer semantic annotations.

### 2.2 Semantic Learning of 3D Scenes

Thanks to the wide availability of various different 3D datasets, a large number of insightful research works have been presented and facilitated. The tremendous progress in semantic learning in turn greatly improved the best performance in several competitive leaderboards. Fundamentally, the semantic learning of 3D point clouds can be attributed to a representation learning problem, and the existing neural architectures can be roughly divided into the following three paradigms:

**1) Voxel-based approaches.** Early works [Le and Duan \(2018\)](#); [Meng et al. \(2019\)](#); [Tchapmi et al. \(2017\)](#) usually voxelize point clouds into dense cubic grids, and then leverage the mature 3D CNN architectures to learn the semantics of each point. Although promising results have been achieved on several benchmarks, these techniques usually require cubically growing computation and memory with the input resolution. This severely limits the application of these methods on large-scale point clouds. To reduce the computational and memory cost, the sparse volumetric representation [Graham et al. \(2018\)](#); [Choy et al. \(2019\)](#); [Cheng et al. \(2021\)](#) and point-voxel joint representation [Liu et al. \(2019\)](#); [Tang et al. \(2020\)](#) are further introduced. Additionally, various different volumetric representations such as spherical voxels [Lei et al.](#)

<sup>1</sup> <https://self-driving.lyft.com/level5/data/>

**Table 1** Comparison with existing representative 3D point cloud datasets. <sup>1</sup>The spatial size (Area/Length) in the dataset, m: meter. Note that, we use distance, instead of area size for outdoor roadway-level datasets. <sup>2</sup>The number of classes used for evaluation and the number of sub-classes annotated in brackets. MLS: Mobile Laser Scanning system, TLS: Terrestrial Laser Scanning system, ALS: Aerial Laser Scanning system. Note that, our dataset has total spatial coverage of 7.6 square kilometers, with nearly 3 billion richly annotated points with 13 semantic categories.

	#Name and Reference	#Year	#Spatial size <sup>1</sup>	#Classes <sup>2</sup>	#Points	#RGB	#Sensors
Object-level	ModelNet Wu et al. (2015)	2015	-	40	-	No	Synthetic
	ShapeNet Chang et al. (2015)	2015	-	55	-	No	Synthetic
	PartNet Mo et al. (2019)	2019	-	24	-	No	Synthetic
	ScanObjectNN Mo et al. (2019)	2019	-	15	-	Yes	RGB-D
Indoor Scene-level	S3DIS Armeni et al. (2017)	2017	$6 \times 10^3 m^2$	13 (13)	273M	Yes	Matterport
	ScanNet Dai et al. (2017)	2017	$1.13 \times 10^5 m^2$	20 (20)	242M	Yes	RGB-D
Outdoor Roadway-level	Paris-rue-Madame Serna et al. (2014)	2014	$0.16 \times 10^3 m$	17	20M	No	MLS
	IQmulus Vallet et al. (2015)	2015	$10 \times 10^3 m$	8 (22)	300M	No	MLS
	Semantic3D Hackel et al. (2017)	2017	-	8 (9)	4000M	Yes	TLS
	Paris-Lille-3D Roynard et al. (2018)	2018	$1.94 \times 10^3 m$	9 (50)	143M	No	MLS
	SemanticKITTI Behley et al. (2019)	2019	$39.2 \times 10^3 m$	25 (28)	4549M	No	MLS
	Toronto-3D Tan et al. (2020)	2020	$1 \times 10^3 m$	8 (9)	78.3M	Yes	MLS
Urban-level	ISPRS Rottensteiner et al. (2012)	2012	-	9	1.2M	No	ALS
	DublinCity Zolanvari et al. (2019)	2019	$2 \times 10^6 m^2$	13	260M	No	ALS
	DALES Varney et al. (2020)	2020	$10 \times 10^6 m^2$	8 (9)	505M	No	ALS
	LASDU Ye et al. (2020)	2020	$1.02 \times 10^6 m^2$	5	3.12M	No	ALS
	Campus3D Li et al. (2020)	2020	$1.58 \times 10^6 m^2$	24	937.1M	Yes	UAV Photogrammetry
	SensatUrban (Ours)	2020	$7.64 \times 10^6 m^2$	13 (31)	2847M	Yes	UAV Photogrammetry

(2020), cylindrical voxels Zhu et al. (2021) are also proposed to adapt to the data distribution of specific point clouds (e.g., LiDAR).

**2) 2D projection-based methods.** Similarly, these pipelines Milioto et al. (2019); Lyu et al. (2020); Cortinhal et al. (2020); Wu et al. (2018a, 2019); Xu et al. (2020) leverage the well-developed 2D CNN frameworks to learn 3D semantics after projecting the point clouds onto 2D images. However, critical geometric information is very likely to be dropped in the 3D-2D projection (e.g., the commonly-used birds-eye-view images), and therefore they are not suitable to learn the relatively small object categories within urban-scale scenarios.

**3) Point-based architectures** Qi et al. (2017a,b); Li et al. (2018); Wang et al. (2019b); Thomas et al. (2019); Hu et al. (2020); Wu et al. (2018b); Yan et al. (2020); Ye et al. (2018); Boulch (2019); Wang et al. (2019a). These methods directly operate on the unstructured point clouds, without relying on any explicit intermediate regular representation. This is achieved by using the simple shared MLPs to learn individual per-point features, and symmetrical aggregation functions to ensure permutation invariance Qi et al. (2017a). In particular, PointNet++ Qi et al. (2017b) is proposed to hierarchically learn the local features, DGCNN Wang et al. (2019b) is introduced to model the topological structure through a graph architecture with Edge-Conv operation. A kernel point convolution Thomas et al. (2019) is proposed to learn spatially correlation in unstructured point clouds. Hu et al. (2020) explore the efficient semantic learning of large-scale point clouds based on the point-based framework. Due to the simple implementation and straightforward architecture, this class of techniques has been widely investigated in several relevant tasks including 3D object detection Zhou and Tuzel (2018); Lang et al. (2019) and instance segmentation Yang

et al. (2019); Jiang et al. (2020). However, it remains unclear whether the existing point pipelines can be well generalized to urban-scale point clouds. To this end, we build our Sensat-Urban dataset and investigate the unique challenges arising from the semantic understanding of urban-scale scenarios.

### 3 Dataset Acquisition and Annotation

In this section, we first describe how we collect (Sec. 3.1) and reconstruct (Sec. 3.2) the urban-scale 3D point clouds using UAV photogrammetry techniques, followed by the detailed procedures to label the dataset over several large urban areas in the UK (Sec. 3.3).



**Fig. 2** The drones and cameras we used in the urban survey.

#### 3.1 Sequential Aerial Imagery Acquisition

Considering the clear advantages of UAV photogrammetry over similar mapping techniques (such as LiDAR) in terms of cost, data quality, and practicality, we adopt a cost-effective fixed-wing mapping drone, Ebee X<sup>2</sup>, equipped with

<sup>2</sup> <https://www.sensefly.com/drone/ebec-x-fixed-wing-drone/>



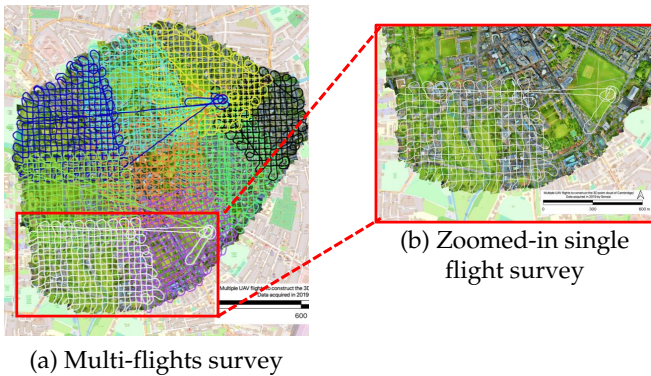


**Fig. 3** An illustration of the survey in a region of Cambridge. A total of 9 flights were carried out together to cover the whole site. Different flight paths of UAVs are represented in lines with different colors. Note that, the drones fly in a grid fashion (*i.e.*, perpendicular flight) to capture more details of the facades of the urban environment. The circular path is the takeoff and landing pattern.

a cutting-edge Sensefly S.O.D.A. camera, to stably capture high-resolution aerial image sequences, as shown in Figure 2. Note that, the camera has the ability to take both oblique and nadir photographs, ensuring that vertical surfaces are captured appropriately. The detailed specification of the camera can be found in Table 2.

In order to fully and evenly cover the survey area, all flight paths are pre-planned in a grid fashion and automated by the flight control system (e-Motion). Several factors have been taken into consideration during the data collection workflow: the area covered, the flying permissions, the level of detail required, and the resolution needed, etc. In light of the limited battery capacity, multiple individual flights are applied in sequence to capture the whole site (each flight lasts between 40-50 minutes). For illustration, Figure 3 shows the paths of the pre-planned multiple flights to cover the selected area in Cambridge city.

These multiple aerial image sequences can then be geo-referenced by Ground Control Points (GCPs) which can be measured by independent professional surveyors with high precision GNSS equipment. Alternatively, the Cambridge data is directly geo-referenced using a highly precise onboard Realtime Kinematic (RTK) GNSS and the final horizontal and vertical RMSEs are  $\pm 50$  mm and  $\pm 75$  mm, respectively (note they can be improved by introducing GCPs). As a comparison, the expected positioning accuracy of point clouds acquired by airborne LiDAR is around 5 to 10 cm, depending on the equipment quality, flying configuration, post-processing, etc. Zhang et al. (2018). The resolution (point density) of our data depends on the number of input images and 3D reconstruction settings. Normally, photogrammetric point clouds are very dense from the process of dense image matching and so need to be subsampled. In our case, all points are subsampled to 2.5 cm, which is denser than most LiDAR data such as DALES Varney et al. (2020).

**Table 2** Detailed specifications of the camera (*i.e.*, Sensefly SODA 3D camera) used in our survey.

		Specification
Sensor size		1 inch
RGB Lens	F/2.8-11, 10.6 mm (35 mm equivalent: 29 mm)	
RGB Resolution		5,472 x 3,648 px (3:2)
Exposure compensation		$\pm 2.0$ (1/3 increments)
Shutter		Global Shutter 1/30 – 1/2000s
White balance		Auto, sunny, cloudy, shady
ISO range		125-6400
RGB FOV	Total FOV: 154°, 64° optical, 90° mechanical	
GNSS		RTK/PPK

### 3.2 Urban-Scale 3D Point Clouds Reconstruction

Our SensatUrban dataset is reconstructed by using the well-established Structure-from-Motion with Multi-View Stereo (SfM-MVS) techniques Westoby et al. (2012) on the highly overlapped 2D aerial image sequences. The camera positions and orientation, and the scene geometry are first recovered simultaneously using a highly redundant iterative bundle adjustment, based on matched features extracted from overlapping offset images. The multi-view stereo image matching technique is then applied to reconstruct dense and coloured 3D point clouds.

In this paper, we use the off-the-shelf software Pix4D<sup>3</sup> to generate the 3D point clouds and orthomosaics. The final outputs of the survey include reconstructed 3D point clouds, 2D orthomosaic images, and 2.5D Digital Surface Model (DSM). In this work, we focus on the 3D point clouds, while the byproduct orthomosaics are only used for visualization purposes. Specifically, we feed all the captured sequential images to Pix4D to generate the 3D point clouds of each region, including the urban area on the periphery of Birmingham, the urban region adjacent to the city centre of Cambridge, and the central area of York. The statistics of the final output point clouds are summarized in Table 3.

**Table 3** Statistics of the reconstructed 3D point clouds in different cities. The area of the surveyed region and the number of generated points are reported.

City	Area ( $km^2$ )	Number of Points
Birmingham	1.2	569,147,075
Cambridge	3.2	2,278,514,725
York	3.2	904,155,619
<b>Total</b>	7.6	3,751,817,419

### 3.3 Point-wise Semantic Annotations

To provide fine-grained information of our dataset for subsequent tasks, we further enrich the reconstructed 3D point clouds with point-wise semantic annotations. However, it

<sup>3</sup> <https://www.pix4d.com/>

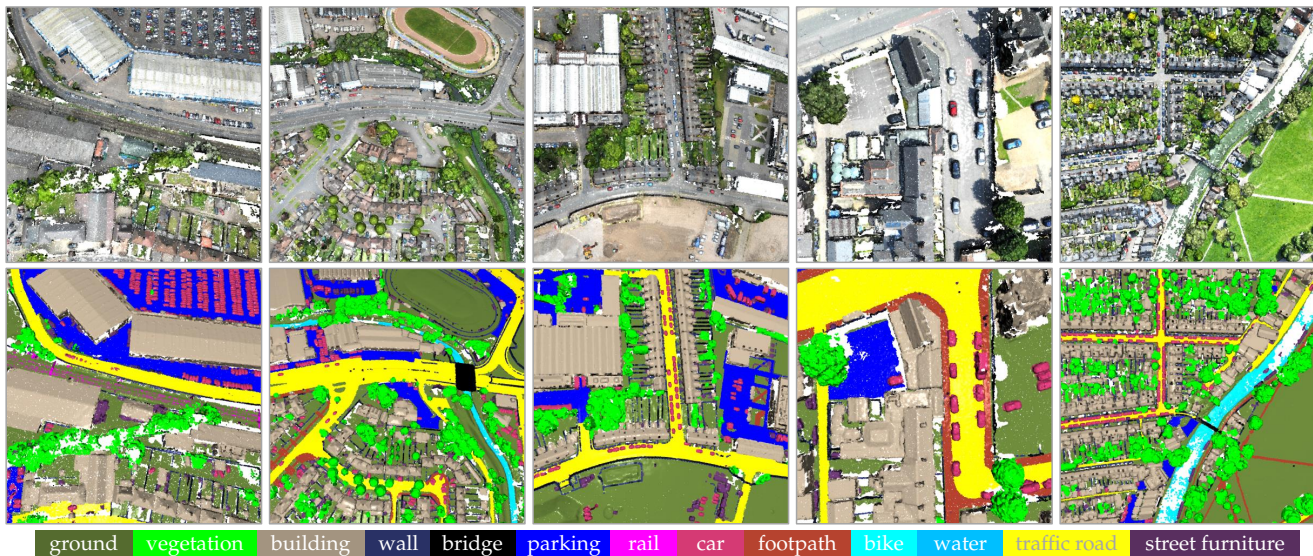


**Fig. 4** Visualization of example point cloud tiles in our SensatUrban dataset. **Top:** the raw point clouds. **Bottom:** the semantic annotations of corresponding point clouds. Points belonging to different semantic categories are displayed in different colors.

is non-trivial and particularly important to decide the categories of interest before manual annotation. In this paper, we specify the semantic categories based on the following three principles: 1) Each annotated category should be of interest to social or commercial purposes, such as asset management Hou et al. (2014), automated structural damage assessment Gerke and Kerle (2011), and urban planning Hu et al. (2003), etc. 2) Each category should have a clear and unambiguous semantic meaning. 3) Different categories should have significant variance in terms of geometric structure or appearance.

Based on these three criteria, we first labeled the point cloud as highly detailed 31 categories via off-the-shelf point cloud labeling tools (*i.e.*, CloudCompare), including fine-grained urban elements such as *benches*, *bollards*, *road signs*, *traffic lights*, etc. Considering the scarcity of data points in certain categories, we merged some similar categories together and finally identified the below 13 semantic classes for all the 3D points in Birmingham and Cambridge. The detailed definition of the semantic categories are shown in Table 4. The points in York remain unlabeled, but made available for possible pre-training in semi-supervised schemes. To ensure the annotation quality, all points are annotated independently by two professional operators in the first round. This is followed by cross-validation in the second round. We also give timely and regular feedback to annotators to address potential issues. All discrepancies in the annotation are carefully addressed, greatly reducing the biases from operators and keeping the annotations consistent and high quality. It takes around 600 working hours to label the entire dataset, and there are no unassigned points discarded in the process. Figure 4 shows examples of our annotations. Table 1 compares the statistics of our SensatUrban with a number of existing 3D datasets.

**Table 4** Class definitions and ordering of our SensatUrban dataset.

Class number	Class name	Definition
1	Ground	impervious surfaces, grass, terrain
2	Vegetation	trees, shrubs, hedges, bushes
3	Building	commercial / residential buildings
4	Wall	fence, highway barriers, walls
5	Bridge	road bridges
6	Parking	parking lots
7	Rail	railroad tracks
8	Traffic Road	main streets, highways, drivable areas
9	Street Furniture	benches, poles, lights
10	Car	cars, trucks, jeeps, SUVs, HGVs
11	Footpath	walkway, alley
12	Bike	bikes / bicyclists
13	Water	rivers / water canals

Note that, our SensatUrban dataset not only incorporates common categories such as *ground*, *building*, and *vegetation*, but also involves several new categories that were not included in the previous urban-scale point cloud datasets Varney et al. (2020); Zolanvari et al. (2019), such as *rail*, *bridge*, and *water*. In particular, these categories are derived by discussing with the industry professionals, and are particularly important for urban planning and infrastructure mapping.

The SensatUrban dataset has been made publicly available<sup>4</sup>, all point clouds and the point-wise ground-truth label of the training set are provided for network training, and an online hidden test set<sup>5</sup> is used to evaluate the final segmentation performance. To prevent overfitting on the test set, the maximum number of submissions is also limited.

<sup>4</sup> <http://point-cloud-analysis.cs.ox.ac.uk>

<sup>5</sup> <https://competitions.codalab.org/competitions/31519>





Fig. 5 Additional examples of our SensatUrban dataset. Different semantic classes are labeled by different colors. The top two rows are point clouds collected from Birmingham, and the bottom two rows are point clouds acquired from Cambridge.

## 4 Benchmarks

### 4.1 Statistics of Train/Val/Test Split

Based on the proposed SensatUrban dataset, we further set up a benchmark to evaluate the performance of existing state-of-the-art segmentation methods. Notably, we first follow DALES Varney et al. (2020) to divide the urban-scale point clouds into similarly sized small tiles (without overlap), so that existing methods can be trained and tested on modern GPUs. Specifically, the urban point clouds collected in Birmingham have been split into 14 tiles, and the Cambridge point clouds are similarly divided into 29 tiles in total. Note that, each tile is approximately  $400 \times 400$  square meters. We also report the detailed statistics of the training/validation/testing subsets in both Birmingham and Cambridge in Figure 6. It

can be seen that the number of points belongs to different semantic categories varies greatly. For example, the dominant three semantic categories, *i.e.*, *ground / building / vegetation*, together account for more than 50% of the total points. However, the minor yet important two categories (*e.g.*, *bike / rail*) only account for 0.025% of the total points. This clearly shows that the class distribution of our SensatUrban dataset is extremely imbalanced, which is in correspondence with the long-tailed distribution of real data. As described in Sec. 4, the imbalanced distribution nature of our dataset also poses great challenges in generalizing the existing segmentation approaches.

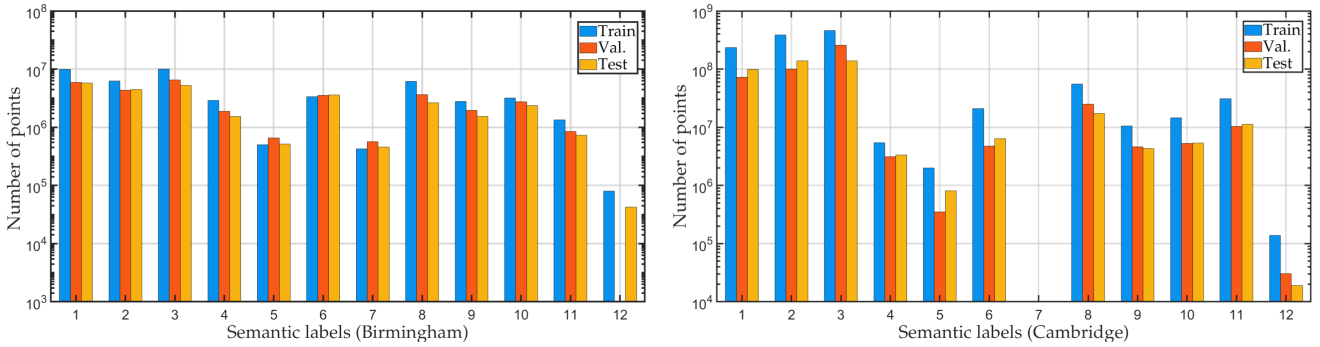


**Fig. 6** Statistics of our SensatUrban labels dataset. The number of points in different semantic categories is reported. Please note that the vertical axis is on the logarithmic scale. Additionally, there are no points annotated as *rail* in Cambridge.

**Table 5** Evaluation of selected baselines on our SensatUrban benchmark. We evaluate on 13 predefined semantic categories using the Overall Accuracy (OA, %), mean class Accuracy (mAcc, %), mean IoU (mIoU, %), and per-class IoU (%).

	OA (%)	mAcc (%)	mIoU (%)	ground	veg.	building	wall	bridge	parking	rail	traffic.	street.	car	footpath	bike	water
PointNet Qi et al. (2017a)	80.78	30.32	23.71	67.96	89.52	80.05	0.00	0.00	3.95	0.00	31.55	0.00	35.14	0.00	0.00	0.00
PointNet++ Qi et al. (2017b)	84.30	39.97	32.92	72.46	94.24	84.77	2.72	2.09	25.79	0.00	31.54	11.42	38.84	7.12	0.00	56.93
TangentConv Tatarchenko et al. (2018)	76.97	43.71	33.30	71.54	91.38	75.90	35.22	0.00	45.34	0.00	26.69	19.24	67.58	0.01	0.00	0.00
SPGraph Landrieu and Simonovsky (2018)	85.27	44.39	37.29	69.93	94.55	88.87	32.83	12.58	15.77	<b>15.48</b>	30.63	22.96	56.42	0.54	0.00	44.24
SparseConv Graham et al. (2018)	88.66	63.28	42.66	74.10	97.90	94.20	63.30	7.50	24.20	0.00	30.10	34.00	74.40	0.00	0.00	54.80
KPConv Thomas et al. (2019)	<b>93.20</b>	63.76	<b>57.58</b>	<b>87.10</b>	<b>98.91</b>	<b>95.33</b>	<b>74.40</b>	28.69	41.38	0.00	55.99	<b>54.43</b>	<b>85.67</b>	<b>40.39</b>	0.00	<b>86.30</b>
RandLA-Net Hu et al. (2020)	89.78	<b>69.64</b>	52.69	80.11	98.07	91.58	48.88	<b>40.75</b>	<b>51.62</b>	0.00	<b>56.67</b>	33.23	80.14	32.63	0.00	71.31

## 4.2 Representative Baselines

To comprehensively evaluate the performance of existing point cloud segmentation pipelines on urban-scale point clouds, we carefully select 7 representative approaches, which cover the three mainstream paradigms as discussed in Section 2.1, as solid baselines in our SensatUrban benchmark. A short summary of these baselines are as follows:

- SparseConvNet Graham et al. (2018). A strong baseline that introduces the submanifold sparse convolutional networks for efficient semantic segmentation of 3D point clouds. This method and its follow-up works Choy et al. (2019); Han et al. (2020) lead the ScanNet benchmark.
- TangentConv Tatarchenko et al. (2018). This method introduces tangent convolution, which operates directly on surface geometry, for large-scale point clouds processing. In particular, the 3D point clouds are first projected as tangent images, followed by 2D convolutional networks.
- PointNet Qi et al. (2017a). This is the pioneering work for directly operating on orderless point clouds by using shared MLPs and symmetrical max-pooling aggregation.
- PointNet++ Qi et al. (2017b). This is the follow-up work of PointNet. It introduced multi-scale/resolution grouping to extract local geometrical patterns, and farthest point sampling to reduce memory and computational cost.
- KPConv Thomas et al. (2019). This approach presents a powerful kernel point convolution to learn spatially correlation from unstructured 3D point clouds. A set of rigid or deformable kernel points are placed to learn varying local

geometries. It has achieved state-of-the-art performance on the aerial DALES dataset Varney et al. (2020).

- SPGraph Landrieu and Simonovsky (2018). This is one of the first learning-based frameworks that capable of processing large-scale point clouds with millions of points. The pipeline composed of geometrically homogeneous partition, followed by superpoint graph construction and contextual segmentation. It is one of the top-performing approaches on the Semantic3D dataset.
- RandLA-Net Hu et al. (2020). It is one of the latest works for efficient semantic understanding of large-scale point clouds. The computational and memory-efficient random sampling, and the hierarchical local feature aggregation are the key to the great performance of this method. It also achieves leading performance on the Semantic3D leaderboard Hackel et al. (2017).

## 4.3 Evaluation Metrics

Similar to most of the existing 3D point cloud benchmarks Hackel et al. (2017); Behley et al. (2019); Armeni et al. (2017), Overall Accuracy (OA), mean class Accuracy (mAcc), and mean Intersection-over-Union (mIoU) are adopted as the primary evaluation criteria of our SensatUrban benchmark. The detailed score of each metric is calculated as follows:

$$OA = \frac{TP}{TP + FP + FN + TN} \quad (1)$$



$$\text{mAcc} = \frac{1}{C} \sum_{c=1}^C \frac{\text{TP}_c}{\text{TP}_c + \text{FN}_c} \quad (2)$$

$$\text{mIoU} = \frac{1}{C} \sum_{c=1}^C \frac{\text{TP}_c}{\text{TP}_c + \text{FP}_c + \text{FN}_c} \quad (3)$$

where TP, TN, FP, FN denote the true-positive, true-negative, false positive, and false negative, separately.  $C$  is the total number of semantic categories. Note that, these scores can also be calculated based on the confusion matrix.

#### 4.4 Benchmark Results

We then evaluate the performance of the aforementioned baselines on our urban-scale SensatUrban dataset. The quantitative results including the per-class IoU scores are reported in Table 5. Note that, we faithfully follow the experimental settings and the publicly available implementation provided by each baseline in their original manuscript. All methods are trained on the same training split for a fair comparison.

Not surprisingly, the performance of all baselines shows varying degrees of degradation, compared with that achieved in other similar aerial point cloud datasets Varney et al. (2020). Specifically, the recent KPConv Thomas et al. (2019) shows the best mIoU performance, but only with a mIoU score of 57.58%, which is still far from satisfactory in practice. In particular, several infrastructure-oriented semantic categories such as *rail*, *footpath*, and *bridge* are poorly segmented. Additionally, we also noticed that the category *bike* is completely misclassified by all baselines. In general, all baselines are more likely to achieve better segmentation performance in categories with simple geometrical structure and dominant proportion, such as *ground*, *vegetation*, *building* and *car*, while achieving relatively limited performance on categories such as *wall*, *bridge*, and *water*. Additionally, different baselines have vastly different performances in individual semantic categories, without a clear leader. Overall, there remain several particular challenges for selected baselines to achieve satisfactory segmentation performance in the proposed city-scale SensatUrban dataset. Motivated by this, we then dive deep into the challenges that arise from our new urban-scale dataset.

## 5 Challenges

In this section, we further analyze the key challenges to generalize existing deep segmentation models to urban-scale photogrammetry point clouds. In particular, we first identify several unique challenges from the perspective of dataset characteristics. Next, we further explore the potential solutions and perform specific experiments to verify the effectiveness. Note that, this paper is not aiming to introduce specific

new algorithms to solve all these challenges, but hopes to point out unresolved issues and provide in-depth analysis and insights, eventually stimulate the development of fine-grained urban-scale point cloud understanding.

### 5.1 Data Preparation

Considering the limited memory of modern GPUs, it is infeasible and unrealistic to directly accommodate and process urban-scale point clouds with billions of points in practice. As a result, the original point cloud data are usually partitioned into small pieces or downsampled before feed into existing neural architectures, so as to find a trade-off between the computational efficiency and segmentation accuracy.

In particular, the early works including PointNet Qi et al. (2017a), PointNet++ Qi et al. (2017b), and their variants usually first divide the large point clouds into equally-sized small blocks with partial overlap (e.g.,  $1\text{m} \times 1\text{m}$  blocks in the S3DIS dataset Armeni et al. (2017)). However, the final segmentation performance is highly-sensitive to the input block size. Large blocks with massive points lead to an unaffordable GPU memory cost, while small blocks inevitably break the objects' geometrical structure. Recent works such as KPConv Thomas et al. (2019) and RandLA-Net Hu et al. (2020) resort to grid or random down-sampling at the beginning to reduce the total amount of points. Additionally, several other works Ye et al. (2018) applied different partitioning or downsampling steps to preprocess the raw point clouds. Overall, various data preparation steps are intensively-involved in existing neural pipelines, but there are still no standard and principled preparation steps in literature, not to mention comprehensive evaluation and analysis.

To further investigate the impact of different data preparations on the final segmentation performance, we standardized a unified two-step data preprocessing framework. The detailed descriptions are as follows:

- Step 1. Reducing the redundant points in the original point clouds through downsampling. This can be achieved by using 1) random downsampling Hu et al. (2020) or 2) grid-downsampling Thomas et al. (2019). In particular, random downsampling has superior computational and memory efficiency, while grid downsampling is robust to varying point densities. Both methods can significantly reduce the total amount of points.
- Step 2. Iteratively feeding mini-batches of point subsets into the network. This can be achieved by first constructing efficient space partitioning data structures such as a KDTree, and then either query 1) constant-number point subsets or 2) constant-volume point subsets from specific regions. In particular, constant-number input sets are usually obtained by querying a fixed number of neighboring points with regard to a specific point Hu et al. (2020),

**Table 6** Semantic segmentation results achieved by selected baselines [Hu et al. \(2020\)](#); [Qi et al. \(2017a\)](#) with different input preparation steps. Note that, the performance of all baselines is evaluated on the original point clouds, instead of a downsampled point cloud.

	Sampling	Input sets	OA(%)	mAcc(%)	mIoU(%)	ground	veg.	building	wall	bridge	parking	rail	traffic.	street.	car	footpath	bike	water
PointNet	Grid	Constant Number	<b>90.57</b>	<b>56.30</b>	<b>49.69</b>	<b>83.55</b>	<b>97.67</b>	90.66	<b>22.56</b>	<b>43.54</b>	40.35	9.29	<b>50.74</b>	<b>29.58</b>	68.24	<b>29.27</b>	0.00	<b>80.55</b>
PointNet	Grid	Constant Volume	88.27	49.80	42.44	80.20	96.43	87.88	8.45	35.14	32.52	0.00	43.03	19.26	54.66	18.26	0.00	75.87
PointNet	Random	Constant Number	90.34	55.17	48.49	83.47	97.51	<b>90.89</b>	18.55	33.31	<b>42.82</b>	<b>11.85</b>	47.95	26.83	<b>68.37</b>	29.12	0.00	79.71
PointNet	Random	Constant Volume	88.09	48.45	41.68	79.82	96.24	87.64	5.69	27.70	34.98	0.00	42.85	13.81	54.29	20.64	0.00	78.24
RandLA-Net	Grid	Constant Number	<b>91.55</b>	<b>74.87</b>	<b>58.64</b>	<b>82.99</b>	<b>98.43</b>	<b>93.41</b>	<b>57.43</b>	<b>49.47</b>	<b>55.12</b>	<b>27.33</b>	<b>60.65</b>	<b>39.43</b>	<b>84.57</b>	<b>39.48</b>	0.00	73.97
RandLA-Net	Grid	Constant Volume	88.11	64.91	49.18	78.18	97.92	90.87	45.02	30.89	35.82	0.00	45.73	31.96	77.78	29.90	0.00	75.30
RandLA-Net	Random	Constant Number	91.14	74.14	57.55	82.25	98.33	92.37	54.20	43.10	54.74	25.02	60.40	39.17	82.77	37.59	0.00	<b>78.25</b>
RandLA-Net	Random	Constant Volume	88.37	60.84	47.27	81.16	97.52	90.45	44.75	16.36	37.18	0.00	42.19	26.28	76.76	30.46	0.00	71.39

while the constant-volume input sets are achieved by cropping fixed-size point cloud chunks (*e.g.*, cubes, spheres) [Qi et al. \(2017a,b\)](#) centered on a specific point. Note that, the query points are random initialized and dynamically updated as in [Thomas et al. \(2019\)](#).

To evaluate the impact of 4 different combinations of both Step 1 and Step 2 on the segmentation performance, we select two representative approaches PointNet [Qi et al. \(2017a\)](#) and RandLA-Net [Hu et al. \(2020\)](#) as the baselines. For a fair comparison, we set the grid size for grid downsampling as 0.2m, while the downsampling ratio is set to 1/10, so as to keep similar number of points after downsampling operation. For constant-number inputs, we implement this by using a pre-built KDTree to query a fixed number of neighboring points of the center point as inputs. For constant volume inputs, we first crop a fixed-size volume (*e.g.*, 8m×8m block) around the center point, followed by random down(up)-sampling to align the number of different input sets.

**Analysis.** Table 6 reports the quantitative semantic segmentation scores achieved by baseline approaches with different input preparations. Table 7 shows the number of points left after downsampling, and the detailed time used for downsampling. It can be seen from the results that:

- Both two baseline approaches consistently show better performance when adopting constant number input sets, compared with corresponding variants which using constant volume input sets.
- Both PointNet and RandLA-Net show slightly better segmentation performance when using grid downsampling at the very beginning, compared with the counterpart using random downsampling. However, the total time consumption for grid downsampling is significantly large than using random downsampling (129s vs. 1107s) when evaluated on the same hardware configuration with an Intel Core™ i9-10900X CPU and an NVIDIA RTX 3090 GPU.

To summarize, our experiments demonstrate the importance of data preparation for the semantic segmentation performance. Although this issue has been overlooked by the community for a long time, we show that the same network architecture can bring up to 10% performance gap, when equipped with different data preparation steps. Therefore, it

**Table 7** Comparison of the grid downsampling and random downsampling at the beginning of data preparation.

	Number of points after sampling	Time consumption(s)
Grid downsample	220,671,929	1107
Random downsample	270,573,783	129

is desirable and encouraged to further investigate the effective data preparation schemes, especially for our urban-scale point cloud datasets.

## 5.2 Geometry vs. Appearance

Different from the point clouds acquired by the airborne LiDAR sensors [Varney et al. \(2020\)](#); [Roynard et al. \(2018\)](#); [Behley et al. \(2019\)](#); [Zolanvari et al. \(2019\)](#), the point clouds in our SensatUrban are colorized with fine-grained point-wise RGB information. Intuitively, the additional color features can provide informative appearance, further enable existing neural architectures to distinguish between heterogeneous semantic categories with similar geometrical structure (*e.g.*, grass on the ground). However, the additional color information may also introduce distractors, which in turn deteriorate the final performance.

Existing techniques usually integrated the RGB color as additional channels of the input feature map feed into the network. However, the recent ShellNet [Zhang et al. \(2019\)](#) learn the semantics from the pure spatial coordinates, but also achieves surprisingly good results. Overall, it remains an open question whether, and how, the color information impacts the final segmentation performance. To this end, we further conduct comparative experiments to verify the impact of the color information to the final segmentation performance. In particular, five baselines including PointNet/PointNet++ [Qi et al. \(2017a,b\)](#), SPGraph [Landrieu and Simonovsky \(2018\)](#), KPConv [Thomas et al. \(2019\)](#), and RandLA-Net [Hu et al. \(2020\)](#) are selected for 10 groups of experiments. Each baseline is trained with the pure geometrical information (*i.e.*, 3D coordinates) or both 3D coordinates and RGB appearance, separately.

**Table 8** Evaluation of semantic segmentation performance of five selected baselines on our SensatUrban dataset with/without the usage of color information.

	OA(%)	mAcc(%)	mIoU(%)	ground	veg.	building	wall	bridge	parking	rail	traffic.	street.	car	footpath	bike	water
PointNet Qi et al. (2017a) (w/o RGB)	83.50	33.52	28.85	67.35	92.66	84.72	16.02	0.00	13.65	2.68	17.09	0.33	54.54	0.00	0.00	26.04
PointNet Qi et al. (2017a) (w/ RGB)	90.57	56.30	49.69	83.55	97.67	90.66	22.56	43.54	40.35	9.29	50.74	29.58	68.24	29.27	0.00	80.55
PointNet++ Qi et al. (2017b) (w/o RGB)	90.85	56.94	50.71	79.05	98.37	94.22	66.76	39.74	37.51	0.00	51.53	38.82	81.71	5.80	0.00	65.68
PointNet++ Qi et al. (2017b) (w/ RGB)	93.10	64.96	58.13	86.38	98.76	94.72	65.91	50.41	50.53	0.00	58.40	46.95	82.31	38.40	0.00	<b>82.88</b>
SPGraph Landrieu and Simonovsky (2018) (w/o RGB)	84.81	42.12	35.29	69.60	94.18	88.15	34.55	20.53	15.83	16.34	31.44	10.54	55.01	0.98	0.00	21.57
SPGraph Landrieu and Simonovsky (2018) (w/ RGB)	85.27	44.39	37.29	69.93	94.55	88.87	32.83	12.58	15.77	15.48	30.63	22.96	56.42	0.54	0.00	44.24
KPConv Thomas et al. (2019) (w/o RGB)	91.47	57.43	51.79	80.43	98.82	94.93	74.17	44.53	32.11	0.00	54.32	37.83	84.88	14.48	0.00	56.79
KPConv Thomas et al. (2019) (w/ RGB)	<b>93.92</b>	71.44	<b>64.50</b>	<b>87.04</b>	<b>99.01</b>	<b>96.31</b>	<b>77.73</b>	<b>58.87</b>	49.88	<b>37.84</b>	<b>62.74</b>	<b>56.60</b>	<b>86.55</b>	<b>44.86</b>	0.00	81.01
RandLA-Net Hu et al. (2020) (w/o RGB)	88.90	67.96	51.53	77.30	97.92	91.24	51.94	47.46	45.04	9.71	49.79	34.21	79.97	21.13	0.00	64.18
RandLA-Net Hu et al. (2020) (w/ RGB)	91.24	<b>74.68</b>	58.14	82.23	98.39	92.69	56.62	49.00	<b>54.19</b>	25.10	60.98	38.69	83.42	38.74	0.00	75.80

**Table 9** Evaluation of semantic segmentation performance of PointNet Qi et al. (2017a) and RandLA-Net Hu et al. (2020) with different loss functions.

	OA(%)	mAcc(%)	mIoU(%)	ground	veg.	building	wall	bridge	parking	rail	traffic.	street.	car	footpath	bike	water
PointNet+ce	<b>90.57</b>	56.30	49.69	<b>83.55</b>	<b>97.67</b>	<b>90.66</b>	22.56	43.54	40.35	9.29	<b>50.74</b>	29.58	<b>68.24</b>	29.27	0.00	<b>80.55</b>
PointNet+wce Hu et al. (2020)	88.13	<b>68.05</b>	51.24	81.01	97.12	87.87	24.46	45.76	47.78	<b>34.93</b>	49.82	29.58	61.28	31.78	0.00	74.67
PointNet+wce+sqrt Aksoy et al. (2019)	89.72	67.97	52.35	82.87	97.33	90.42	28.32	44.94	48.39	32.07	49.58	<b>32.63</b>	65.11	32.59	<b>2.60</b>	73.71
PointNet+lovass Berman et al. (2018)	89.58	67.50	<b>52.53</b>	82.74	97.27	90.28	28.11	43.89	<b>48.53</b>	33.58	49.68	32.21	64.01	<b>33.05</b>	1.46	78.13
PointNet+focal Lin et al. (2017)	89.46	67.33	52.37	82.47	97.34	90.25	<b>28.36</b>	<b>51.87</b>	46.40	30.50	48.62	32.43	65.00	32.23	1.21	74.10
RandLA-Net+ce	<b>93.10</b>	64.30	57.77	<b>85.39</b>	<b>98.63</b>	<b>95.40</b>	62.55	54.85	56.49	0.00	58.13	<b>45.90</b>	82.24	30.68	0.00	80.70
RandLA-Net+wce Hu et al. (2020)	91.24	74.68	58.14	82.23	98.39	92.69	56.62	49.00	54.19	25.10	<b>60.98</b>	38.69	83.42	38.74	0.00	75.80
RandLA-Net+wce+sqrt Aksoy et al. (2019)	92.51	<b>79.92</b>	<b>62.80</b>	84.94	98.47	95.07	59.01	<b>62.18</b>	56.76	28.96	57.36	44.47	<b>84.67</b>	41.67	<b>24.31</b>	78.49
RandLA-Net+lovass Berman et al. (2018)	92.56	76.99	61.51	84.92	98.55	94.64	<b>63.17</b>	52.37	55.43	<b>36.37</b>	59.35	45.79	84.28	41.24	2.66	<b>80.89</b>
RandLA-Net+focal Lin et al. (2017)	92.49	77.26	60.41	85.03	98.38	94.74	59.49	58.70	<b>57.11</b>	25.97	58.19	42.74	82.26	<b>42.00</b>	2.71	77.97

**Analysis.** We report the quantitative results achieved by the selected five baselines with/without the usage of color in the input point clouds. We can see that:

- All of PointNet/PointNet++, KPConv, and RandLA-Net achieve significant performance improvement when the color features are utilized, compared with the use geometrical coordinates alone. It is noted that categories with significant performance improvements include *bridge*, *footpath*, and *water*, since these categories are geometrically indistinguishable.
- We also noticed that the performance improvement of SPGraph is relatively marginal (only 2%) compared with other baseline approaches. This is likely due to the homogenous geometrical partition used in its framework, which purely relies on the geometrical structure but ignores the informative color.

Apart from the quantitative results, we also explicitly visualize the qualitative results achieved by these baselines in Figure 7. To summarize, our experiments highlight the importance of color information to the fine-grained understanding of urban-scale point clouds, reflecting the advantages of our SensatUrban dataset over other existing aerial point clouds datasets collected by LiDAR, such as DALES Varney et al. (2020), NPM3D Roynard et al. (2018), and DublinCity Zolanvari et al. (2019). In particular, the color information is particularly important for distinguishing heterogeneous categories with consistent geometric structures (e.g., grass on the road), enabling a higher level of semantic

understanding. This also provides insights for future aerial mapping campaigns, where color information and even other spectral bands may be useful for the semantic understanding.

### 5.3 The Impact of Skewed Class Distribution

Although data preparations and the usage of color information have been considered, it is still noted that the performance of different semantic categories varies greatly. For example, all baseline methods can achieve excellent segmentation performance on *vegetation*, with IoU scores up to 99%, while completely failed in detecting rare patterns such as *bikes*. Fundamentally, this is because of the extremely imbalanced distribution of our dataset. As illustrated in Figure 6, the SensatUrban dataset is dominated by categories such as *ground/vegetation/building*, which are commonly appeared in urban areas of modern cities. However, categories such as *rail/bike*, despite being highly important for infrastructure-oriented applications, occurring much less frequently than the prevalent categories. As consequence, the selected baselines show a biased tendency towards the prevalent categories during inference, due to the scarce occurrence of the under-represented categories.

It remains an open question to learn from training data with skewed distributions. In this paper, we attempt to alleviate this problem from the perspective of the loss function. In particular, advanced loss functions are utilized to adaptively re-weight the contributions of each point that belongs

**Table 10** Cross-city generalization performance of selected baselines on our SensatUrban dataset. All baselines are trained on the *training split of Birmingham*. The top five records show the testing results on the *testing split of Birmingham*, while the bottom five rows show the scores on the *testing split of Cambridge (cross-city)*.

	OA(%)	mAcc(%)	mIoU(%)	ground	veg.	building	wall	bridge	parking	rail	traffic.	street.	car	footpath	bike	water
PointNet Qi et al. (2017a)	87.33	54.76	48.73	80.91	94.58	87.40	33.69	0.51	66.23	16.98	49.55	36.08	74.59	1.49	0.00	91.51
PointNet++ Qi et al. (2017b)	89.85	64.24	57.39	84.34	97.11	89.74	61.56	<b>3.78</b>	68.08	41.95	54.43	51.54	84.73	14.43	0.00	<b>94.34</b>
SPGraph Landrieu and Simonovsky (2018)	80.13	42.87	36.95	65.75	93.33	87.24	41.28	0.00	42.69	20.94	2.28	32.05	64.06	0.00	0.00	30.76
KPConv Thomas et al. (2019)	<b>91.44</b>	68.41	<b>61.65</b>	<b>86.00</b>	<b>97.66</b>	<b>92.90</b>	<b>75.07</b>	0.91	<b>69.74</b>	<b>55.50</b>	<b>57.94</b>	<b>60.73</b>	<b>89.48</b>	21.44	0.00	94.13
RandLA-Net Hu et al. (2020)	90.77	<b>72.11</b>	59.72	85.14	96.89	90.77	59.45	1.52	75.83	48.88	62.58	48.65	86.31	<b>28.82</b>	0.00	91.51
PointNet Qi et al. (2017a)	86.06	38.56	29.70	74.94	94.57	85.38	8.62	13.42	16.47	0.00	38.64	14.27	36.96	0.09	0.00	2.75
PointNet++ Qi et al. (2017b)	89.46	44.64	36.93	77.68	97.28	91.95	54.59	0.52	15.84	0.00	42.08	29.00	67.71	0.24	0.00	3.16
SPGraph Landrieu and Simonovsky (2018)	82.02	24.83	20.70	61.72	88.26	78.27	8.29	0.00	0.00	0.00	0.64	1.87	30.00	0.00	0.00	0.00
KPConv Thomas et al. (2019)	<b>90.62</b>	48.71	<b>40.51</b>	<b>78.88</b>	<b>98.33</b>	<b>94.24</b>	<b>76.20</b>	0.01	14.70	0.00	41.77	<b>39.32</b>	<b>74.22</b>	0.39	0.00	<b>8.61</b>
RandLA-Net Hu et al. (2020)	88.92	<b>51.57</b>	40.29	78.46	97.12	89.93	46.77	<b>28.76</b>	<b>20.03</b>	0.00	<b>46.98</b>	18.70	65.99	<b>24.91</b>	0.00	6.15

**Table 11** Cross-city generalization performance of selected baselines on our dataset. All baselines are trained on the *training split of Cambridge*. The top five records show the testing results on the *testing split of Cambridge*, while the bottom five rows show the scores on the *testing split of Birmingham (cross-city)*.

	OA(%)	mAcc(%)	mIoU(%)	ground	veg.	building	wall	bridge	parking	rail	traffic.	street.	car	footpath	bike	water
PointNet Qi et al. (2017a)	91.16	50.02	43.61	82.83	97.89	90.93	9.54	38.34	12.07	0.00	50.60	21.42	60.74	26.18	0.00	76.42
PointNet++ Qi et al. (2017b)	93.62	62.64	55.60	85.50	98.93	95.35	63.73	59.19	24.00	0.00	59.13	40.50	79.30	38.01	0.00	79.11
SPG Landrieu and Simonovsky (2018)	84.13	36.36	31.55	68.96	92.14	84.61	15.37	13.84	4.46	0.00	31.83	21.02	22.04	0.47	0.00	23.83
KPConv Thomas et al. (2019)	<b>94.89</b>	<b>69.65</b>	<b>62.36</b>	<b>87.91</b>	<b>99.22</b>	<b>97.00</b>	<b>80.09</b>	<b>77.31</b>	<b>36.65</b>	0.00	<b>65.62</b>	<b>54.70</b>	<b>84.59</b>	<b>43.25</b>	<b>0.00</b>	<b>84.34</b>
RandLA-Net Hu et al. (2020)	91.45	69.55	53.21	81.39	98.49	93.43	56.40	49.40	35.80	0.00	60.75	31.29	81.11	37.20	0.00	66.55
PointNet Qi et al. (2017a)	71.99	43.90	35.01	64.55	93.76	72.71	5.30	17.55	8.08	0.00	26.60	8.87	65.35	11.34	0.00	<b>80.99</b>
PointNet++ Qi et al. (2017b)	78.47	52.32	41.29	70.52	96.07	70.13	44.89	6.60	34.67	0.00	33.39	27.42	73.79	16.78	0.00	62.48
SPG Landrieu and Simonovsky (2018)	71.27	28.42	22.93	57.32	84.28	76.51	12.40	8.95	0.00	0.00	20.41	10.52	14.08	0.00	0.00	13.65
KPConv Thomas et al. (2019)	<b>86.03</b>	<b>61.76</b>	<b>50.67</b>	<b>78.46</b>	<b>97.20</b>	81.72	<b>55.76</b>	<b>40.08</b>	<b>64.05</b>	0.00	<b>44.99</b>	<b>38.91</b>	<b>80.01</b>	<b>17.79</b>	<b>0.00</b>	59.76
RandLA-Net Hu et al. (2020)	75.52	59.27	40.08	63.42	93.12	73.54	44.09	5.35	45.54	0.00	31.68	25.66	74.47	8.93	0.00	55.25

to different categories, eventually guiding the network to achieve a more balanced performance across different categories. Specifically, by taking PointNet and RandLA-Net as baselines, we replace the original vanilla cross-entropy loss with four off-the-shelf loss functions, including weighted cross-entropy with inverse frequency Cortinhal et al. (2020), or with inverse square root (sqrt) frequency Rosu et al. (2019), Lovász-softmax loss Berman et al. (2018), and focal loss Lin et al. (2017).

**Analysis.** We report the detailed segmentation performance of two baselines achieved with five different loss functions. We can see the performance of all baselines has been improved when advanced loss functions are adopted. This clearly demonstrated that the sophisticated loss functions are indeed effective to alleviate the problem of imbalanced class distribution. Notably, we also noticed that the mIoU score of RandLA-Net has been improved by 5% when using the weighted cross-entropy loss. In particular, the score in the most under-represented category bike has been improved by more than 20%. Although the performance on minority categories is still far from satisfactory, the improvement is considerably encouraged and we suggest that more research could be conducted on this challenge, so as to fully tackle this research problem.

## 5.4 Cross-City Generalization

One of the main challenges of existing deep neural architectures is how to enhance the generalization capability to unseen scenarios, especially out-of-distribution data, since neural networks are usually data hungry and tend to overfit the training data. Motivated by this, we further explore the generalization performance of existing representative baselines on our SensatUrban dataset, since our dataset is composed of data collected from different cities, hence naturally suitable for evaluation the generalization abilities. In particular, five baseline approaches are included in our generalization experiments, that is: PointNet/PointNet++ Qi et al. (2017a,b), SPGraph Landrieu and Simonovsky (2018), KPConv Thomas et al. (2019), and RandLA-Net Hu et al. (2020). The detailed four groups of experimental schemes are described as follows:

- Group 1: Train Birmingham/Test Birmingham. All of the five baseline approaches are only trained and tested on the training split and test split of Birmingham, respectively.
- Group 2: Generalize from Birmingham to Cambridge: All of the five baselines are trained on the training split of Birmingham, and tested on the testing split of Cambridge.
- Group 3: Train Cambridge/Test Cambridge: Analogous to group 1, all of the 5 baselines are only trained on the



training split of Cambridge, and then tested on the testing split of the same region.

- Group 4: Generalize from Cambridge to Birmingham: the above well-trained 5 baseline models in group 3 are directly tested on the testing split of Birmingham.

**Analysis.** We report the detailed results achieved in the first two groups of experiments in Table 10, and the last two groups of experiments in Table 11. It can be seen that the performance of all baselines shows a significant decrease (approximate 20% drop on average in mIoU scores) when generalizing the trained model to unseen urban areas in other cities, despite the data collected from different cities are actually in the same domain (*i.e.*, captured using the same sensor). This demonstrates the limited generalization capacity of selected baseline approaches. Interestingly, we also noticed that the performance of dominant semantic categories such as *vegetation* and *building* are not severely affected, while the under-presented categories including *rail* and *water* show visible performance degradation. This shows the baseline approaches are actually overfitted to the prevalent categories, while they failed to learn generalized and meaningful representation for minority categories. Overall, generalizing the trained deep segmentation model to unseen data, especially point clouds with different distributions, remains an open question in this area. Therefore, we hope our SensatUrban dataset could highlight the limited generalization capacity of existing deep neural architectures, and inspire more research to be conducted on this challenging problem.

**Table 12** The class mapping from DALES and SensatUrban dataset to the final unified semantic categories.

Classes of DALES	Mapped class	Classes of SensatUrban
Ground	Ground	Ground, Bridge, Parking, Rail, Traffic Road, Footpath
Vegetation	Vegetation	Vegetation
Cars, Trucks	Cars	Cars
Power lines, Poles	Street furniture	Street furniture
Fences	Fences	Walls
Buildings	Buildings	Buildings
Unclassified	Unclassified (Ignored)	Bikes, Waters

**Table 13** Statistics of the DALES dataset and SensatUrban dataset after class mapping.

Mapped classes	DALES		SensatUrban	
	Training	Test	Training	Test
Ground	178,021,561	68,871,897	667,443,997	188,848,584
Vegetation	120,818,120	41,464,228	544,284,286	158,512,452
Cars	3,332,171	1,224,696	37,557,130	10,918,466
Street furniture	1,076,810	323,136	26,669,467	6,656,919
Fences	1,512,927	624,069	20,606,217	5,682,668
Buildings	56,908,533	23,454,294	861,977,674	164,867,233
Unclassified	6,997,560	681,571	7,262,966	4,449,979

## 5.5 Cross-Dataset Generalization

Another interesting question is whether the deep model trained on our SensatUrban dataset can be well generalized to other similar airborne point cloud datasets Varney et al. (2020); Zolanvari et al. (2019), or vice versa. Intuitively, this task seems even more challenging than cross-city generalization, since the point clouds acquired from different cities in our dataset are inherently homogeneous. That is, the point cloud is reconstructed from sequential aerial images captured by the same camera, with the identical data process pipeline. However, point clouds in different datasets are likely to be collected by distinct acquisition sensors (*i.e.*, airborne LiDAR vs. photogrammetry camera) and generated by using different mapping techniques. Moreover, the data distribution, point density, geographic regions, scene contents and annotation practices may vary greatly. Albeit interesting, there are few relevant studies in the field of 3D point cloud semantic understanding.

In this paper, we move a step forward to explore how the domain shift in different datasets affects the semantic learning of deep neural networks. Specifically, we select the recent aerial LiDAR point clouds dataset DALES Varney et al. (2020), along with the proposed photogrammetry SensatUrban dataset, to evaluate the cross dataset generalization capacity of existing segmentation algorithms. Note that, due to the inconsistent taxonomies and annotation practice, the semantic categories (*i.e.*, 8 valid categories in DALES vs. 13 valid categories in SensatUrban) and definitions are different in these two datasets. Therefore, we first reconcile the taxonomies and map the semantic categories into the newly defined 6 consistent semantic categories, so as to properly evaluate the generalization performance across datasets. The detailed class mapping from each dataset to the unified taxonomy is shown in Table 12. The statistics (*i.e.*, the number of points in the training and test subset) after class mapping is reported in Table 13. It can be seen that the class distribution of the two datasets exhibits visible differences. Here, we select the representative PointNet and RandLA-Net as the baselines, for the evaluation of intra-dataset generalization, and cross-dataset generalization performance. Note that, the baseline approaches are trained with the usage of 3D spatial coordinates only, since the color information is not available in LiDAR point clouds provided by the DALES dataset.

**Analysis.** We can see that: 1) RandLA-Net has achieved superior performance in the intra-dataset evaluation, since the overall difficulty is reduced after the class mapping. 2) Although we considered the point density and the number of input points during data preprocessing, the cross-dataset generalization performance of both two baseline approaches is still significantly lower than the intra-dataset evaluation (30%+), demonstrating that domain shifts in different datasets play a key role in preventing model generalization. Future studies

**Table 14** Quantitative cross-dataset generalization results were achieved by the selected baseline approaches on the proposed SensatUrban dataset and the DALES dataset.

Methods	Settings	OA(%)	mIoU(%)	Ground	Vegetation	Cars	Street furniture	Fences	Buildings
PointNet Qi et al. (2017a)	DALES → DALES	94.10	59.72	94.68	86.69	16.48	73.62	0.00	86.87
	DALES → SensatUrban	74.25	30.75	89.44	55.69	0.02	0.03	0.00	39.32
	SensatUrban → SensatUrban	92.46	56.27	92.90	92.14	52.69	0.33	14.25	85.33
	SensatUrban → DALES	87.45	41.98	92.64	72.15	2.77	11.79	8.31	64.23
RandLA-Net Hu et al. (2020)	DALES → DALES	96.98	84.31	96.99	92.71	80.54	89.08	50.09	96.47
	DALES → SensatUrban	83.69	40.69	93.02	64.03	0.25	0.23	16.63	69.96
	SensatUrban → SensatUrban	96.55	79.47	96.87	98.28	80.44	45.18	60.92	95.16
	SensatUrban → DALES	84.25	43.57	92.63	66.26	27.33	2.27	8.89	64.07

are encouraged to further reduce the domain gap between different point cloud datasets, especially in light of the different configurations of existing LiDAR point clouds.

### 5.6 Semantic Learning with Fewer Labels

Deep learning-based methods are hungry for massive training data Wei et al. (2020). For fully-supervised segmentation pipelines such as Hu et al. (2020); Thomas et al. (2019); Qi et al. (2017a,b), a large amount of fine-grained per-point annotations are usually required. However, it is extremely time-consuming and labor-intensive to manually annotate an urban-scale point cloud dataset with thousands of millions of points in practice. To this end, we further investigate the possibility of semantic learning with limited annotations on our SensatUrban dataset.

Inspired by the weak supervision setting proposed in Xu and Lee (2020), we have conducted six groups of experiments by training all baselines with different forms of semantic annotations (*i.e.*, weak supervisions) in our dataset. For simplicity, we only adopt PointNet Qi et al. (2017a), PointNet++ Qi et al. (2017b) and RandLA-Net Hu et al. (2020) as baseline networks in the following groups of experiment:

- Only 1 point annotated per category in each point cloud.
- Only 1% points annotated per category in each point cloud.
- Only 1% points annotated in each point cloud (randomly).
- 10% points annotated per category in each point cloud.
- 10% points annotated in each point cloud (randomly).
- 100% (all) points annotated in each point cloud.

**Analysis.** Table 15 shows the detailed quantitative results achieved by three baselines under different settings. It can be seen that:

- Surprisingly, both PointNet, PointNet++, and RandLA-Net can achieve comparable performance with their fully-supervised counterpart, even when training with a small fraction of labeled points (*e.g.*, 1% or 10%). This implies that the existing per-point annotations may exist large information redundancy, it is possible to learn semantics with limited annotations.
- The performance of all baselines in group 2 and group 4 are better than group 3 and group 5, demonstrating that

randomly annotating a tiny fraction (*e.g.*, 1%, 10%) of all points is inferior to randomly annotating a tiny fraction of points in each semantic category. Although randomly annotating a tiny fraction of all points is more practical and feasible.

- The segmentation performance of all baselines in group 1 (*i.e.*, with 1 point annotation) are far from satisfactory. Basically, the networks cannot converge, primarily because the supervision information is extremely insufficient. However, this is also one of the simplest and cheapest ways of annotation in practice. More studies should be conducted in this direction to further improve the performance.

Thanks to the availability of several large-scale point cloud datasets, the community can always assume that the amount of labeled training data is sufficient. However, we have demonstrated that comparable performance can also be achieved using the same architecture with limited semantic annotations, highlighting the great potential of weakly-supervised semantic segmentation frameworks. This motivates us to further investigate how to achieve better performance under limited annotation, and how to choose the best annotation strategy under fixed budgets.

### 5.7 Self-supervised Pre-Training on 3D Point Clouds

Pre-training a network on a rich source set in a self-supervised or unsupervised way has been demonstrated to be highly effective for high-level downstream tasks (*e.g.*, segmentation, detection) in several 2D vision tasks Chen et al. (2020); He et al. (2020). However, self-supervised pre-training on 3D point clouds is still in its infancy, only a handful of recent works Sauder and Sievers (2019); Wang et al. (2020); Xie et al. (2020); Zhang et al. (2021); Hou et al. (2020); Poursaeed et al. (2020) have started to explore self-supervised learning on unstructured 3D point clouds. In particular, all existing methods are still pre-trained on the object-level datasets (*e.g.*, ModelNet40 Wu et al. (2015)) or indoor scene-level datasets (*e.g.*, ScanNet Dai et al. (2017)). Considering the urban-scale property of SensatUrban, it is particularly suitable for verifying the effectiveness of the existing pretraining strategy on our dataset.

**Table 15** Quantitative results achieved by PointNet Qi et al. (2017a), PointNet++ Qi et al. (2017b), and RandLA-Net Hu et al. (2020) with different settings (varying number of semantic annotations). † means randomly a tiny fraction points of each semantic category, ‡ means randomly a tiny fraction points of the whole points.

Settings	Methods	OA(%)	mAcc(%)	mIoU(%)	ground	veg.	building	wall	bridge	parking	rail	traffic.	street.	car	footpath	bike	water
1 pt	PointNet	42.30	13.12	7.90	13.79	45.84	36.53	0.36	0.00	2.49	0.00	0.00	1.58	1.98	0.09	0.00	0.00
	PointNet++	29.52	20.82	8.74	21.48	24.52	24.80	1.81	0.00	8.99	0.00	15.56	3.52	5.91	7.02	0.02	0.03
	RandLA-Net	1.97	14.07	1.93	0.00	0.00	0.00	1.31	0.59	7.92	0.30	0.02	1.17	1.00	7.84	0.01	4.94
1% annotation† per category	PointNet	89.58	52.87	45.95	82.92	97.40	90.07	16.12	28.83	33.82	5.86	44.95	26.98	65.50	23.15	0.00	81.81
	PointNet++	91.70	59.21	52.05	85.42	98.67	93.96	59.48	24.50	37.21	0.00	49.45	39.23	78.91	30.04	0.00	79.76
	RandLA-Net	91.18	71.76	55.80	82.07	98.26	94.12	54.04	55.28	55.25	0.01	57.55	40.47	83.51	35.47	0.00	69.40
1% annotation‡	PointNet	89.11	50.25	43.46	82.33	97.13	89.20	11.12	15.92	34.38	0.00	42.33	23.63	63.73	26.33	0.00	78.94
	PointNet++	91.75	58.31	51.49	83.90	98.58	94.16	60.96	13.74	41.71	0.00	50.74	40.64	78.71	24.80	0.00	81.39
	RandLA-Net	90.53	69.92	54.21	81.03	98.26	93.32	53.24	53.61	50.36	0.00	54.31	37.87	82.77	34.47	0.00	65.50
10% annotation† per category	PointNet	89.67	53.73	47.31	81.82	97.49	89.70	18.83	43.13	30.20	9.48	47.62	29.39	64.77	25.21	0.00	77.39
	PointNet++	92.60	63.24	56.67	86.08	98.73	94.65	64.68	49.87	43.77	0.00	53.70	45.51	82.29	36.20	0.00	81.27
	RandLA-Net	91.59	72.92	57.44	83.07	98.18	93.48	51.25	<b>54.77</b>	<b>58.32</b>	12.72	<b>62.06</b>	38.81	<b>83.82</b>	<b>39.42</b>	0.00	70.79
10% annotation‡	PointNet	88.64	51.51	43.78	81.80	97.26	88.51	16.97	33.58	16.67	1.27	43.30	24.44	65.37	24.14	0.00	75.77
	PointNet++	92.28	60.71	53.84	85.39	98.64	94.13	60.59	25.89	46.15	0.00	53.34	42.73	80.78	30.04	0.00	82.19
	RandLA-Net	89.91	69.80	52.15	79.73	97.91	93.04	54.08	44.06	50.68	0.00	53.87	35.52	81.72	30.58	0.00	56.75
Full supervision	PointNet	90.57	56.30	49.69	83.55	97.67	90.66	22.56	43.54	40.35	9.29	50.74	29.58	68.24	29.27	0.00	80.55
	PointNet++	<b>93.10</b>	64.96	58.13	<b>86.38</b>	<b>98.76</b>	<b>94.72</b>	<b>65.91</b>	50.41	50.53	0.00	58.40	<b>46.95</b>	82.31	38.40	0.00	<b>82.88</b>
	RandLA-Net	91.24	<b>74.68</b>	<b>58.14</b>	82.23	98.39	92.69	56.62	49.00	54.19	<b>25.10</b>	60.98	38.69	83.42	38.74	0.00	75.80

**Table 16** Quantitative results achieved by using OcCo Wang et al. (2020), Jigsaw Sauder and Sievers (2019) and Random (Rand) initialization on the SensatUrban dataset, based on PointNet Qi et al. (2017a), PCN Yuan et al. (2018) and DGCNN Wang et al. (2019b) encoders. Note that, all the initialized weights are obtained by pre-training on the ModelNet40 Wu et al. (2015), since these techniques are mainly designed for object-level classification and segmentation.

		OA(%)	mAcc(%)	mIoU(%)	ground	veg.	building	wall	bridge	parking	rail	traffic.	street.	car	footpath	bike	water
PointNet	Qi et al. (2017a)	86.29	53.33	45.10	80.05	93.98	87.05	23.05	19.52	41.80	3.38	43.47	24.20	63.43	26.86	0.00	79.53
	Sauder and Sievers (2019)	87.38	56.97	47.90	83.36	94.72	88.48	22.87	30.19	47.43	15.62	44.49	22.91	64.14	30.33	0.00	77.88
	Wang et al. (2020)	87.87	56.14	48.50	83.76	94.81	89.24	23.29	33.38	48.04	15.84	45.38	24.99	65.00	27.13	0.00	79.58
PCN	Yuan et al. (2018)	86.79	57.66	47.91	82.61	94.82	89.04	26.66	21.96	34.96	28.39	43.32	27.13	62.97	30.87	0.00	80.06
	Sauder and Sievers (2019)	87.32	57.01	48.44	83.20	94.79	89.25	25.89	19.69	40.90	28.52	43.46	24.78	63.08	31.74	0.00	<b>84.42</b>
	Wang et al. (2020)	86.90	58.15	48.54	81.64	94.37	88.21	25.43	31.54	39.39	22.02	45.47	27.60	65.33	32.07	0.00	77.99
DGCNN	Wang et al. (2019b)	87.54	60.27	51.96	83.12	95.43	89.58	<b>31.84</b>	35.49	45.11	38.57	45.66	32.97	64.88	30.48	0.00	82.34
	Sauder and Sievers (2019)	88.65	60.80	53.01	<b>83.95</b>	<b>95.92</b>	89.85	30.05	<b>43.59</b>	46.40	35.28	49.60	31.46	69.41	<b>34.38</b>	0.00	80.55
	Wang et al. (2020)	<b>88.67</b>	<b>61.35</b>	<b>53.31</b>	83.64	95.75	<b>89.96</b>	29.22	41.47	<b>46.89</b>	<b>40.64</b>	<b>49.72</b>	<b>33.57</b>	<b>70.11</b>	32.35	0.00	79.74

To this end, we conducted three groups of experiments on our SensatUrban dataset to compare the performance of:

- Pre-training with occlusion completion Wang et al. (2020).
- Pre-training with context prediction (jigsaw) Sauder and Sievers (2019).
- Training from scratch.

For simplicity, we faithfully follow the three baseline networks used in their original paper Wang et al. (2020); Sauder and Sievers (2019), including PointNet Qi et al. (2017a), PCN Yuan et al. (2018), and DGCNN Wang et al. (2019b). The detailed experimental results are shown in Table 16.

**Analysis.** From the results in Table 16 we can see that, although both baseline networks are purely pre-trained on the object-level point clouds in ModelNet40, the fine-tuning models can still achieve a certain performance improvement on our dataset. In particular, the performance of several minority categories, such as *rail* and *bridge*, has a significant performance improvement (up to nearly 10%), primary because the pre-trained models are less prone to overfitting to the majority categories, compared to directly training from scratch.

This further demonstrates the feasibility and potential of the self-supervised pre-training paradigm. However, the existing pre-training framework Wang et al. (2020); Sauder and Sievers (2019) are still limited to object-level point clouds, and it is non-trivial to be extended to large-scale point clouds. On the other hand, most of the existing pre-training schemes are based on auxiliary (pre-text) tasks. It is worth investigating how to leverage contrastive learning to achieve better performance on 3D point clouds. Finally, to further facilitate the research in this research area, we also release the unlabeled York point clouds, encouraging further research exploration on this part of the data.

## 6 Discussion and Limitations

Although the proposed SensatUrban dataset is currently the largest publicly available photogrammetric point cloud dataset, it is not without limitation. In general, instance annotation would be a meaningful addition to our dataset. However, due to the tremendous labeling effort of point-wise instance labels, we leave the integration of instance labels for future

exploration. On the other hand, our dataset is reconstructed from the sequential aerial images captured by a single sensor (*i.e.*, camera), it would be interesting to further investigate the same-source data acquired by different sensors. For example, the data acquired from both a camera and a LiDAR system integrated on the same UAV platform [Kölle et al. \(2021\)](#).

## 7 Summary and Outlook

This paper introduces SensatUrban: an urban-scale photogrammetric point cloud dataset composed of  $7.6 \text{ km}^2$  of urban areas in three UK cities, and nearly 3 billion richly annotated points (each with one of the 13 semantic categories). A comprehensive benchmark is also built based on this dataset and a number of selected representative baselines. In particular, extensive comparative experiments have revealed several challenges in generalizing existing semantic segmentation methods to urban-scale point clouds, including how to conduct data preparation, whether and how to utilize the color information, how to tackle with the extremely imbalanced class distribution, generalizing to unseen scenarios, and the potential of weakly/self-supervised learning techniques. Besides, extensive benchmarking results are conducted and in-depth analysis are also provided. In the future, we will further increase the scale and richness (*i.e.*, instance annotation, corresponding 2D images) of our SensatUrban dataset. We hope that our SensatUrban dataset could be an immensely useful resource and a canonical benchmark to related research communities including 3D computer vision, earth vision and remote sensing, inspiring and supporting future advancing research in related areas.

**Acknowledgements** This work was supported by a China Scholarship Council (CSC) scholarship, Huawei UK AI Fellowship, and the UKRI Natural Environment Research Council (NERC) Flood-PREPARED project (NE/P017134/1). Bo Yang was partially supported by HK PolyU (P0034792) and Shenzhen Science and Technology Innovation Commission (JCYJ20210324120603011). The authors highly appreciate the Data Study Group (DSG) organised by the Alan Turing Institute and the GPU resources generously provided by the LAVA group led by Professor Yulan Guo in the Sun Yat-sen University, China. The authors would also like to thank the pre-training results provided by Hanchen Wang from the University of Cambridge.



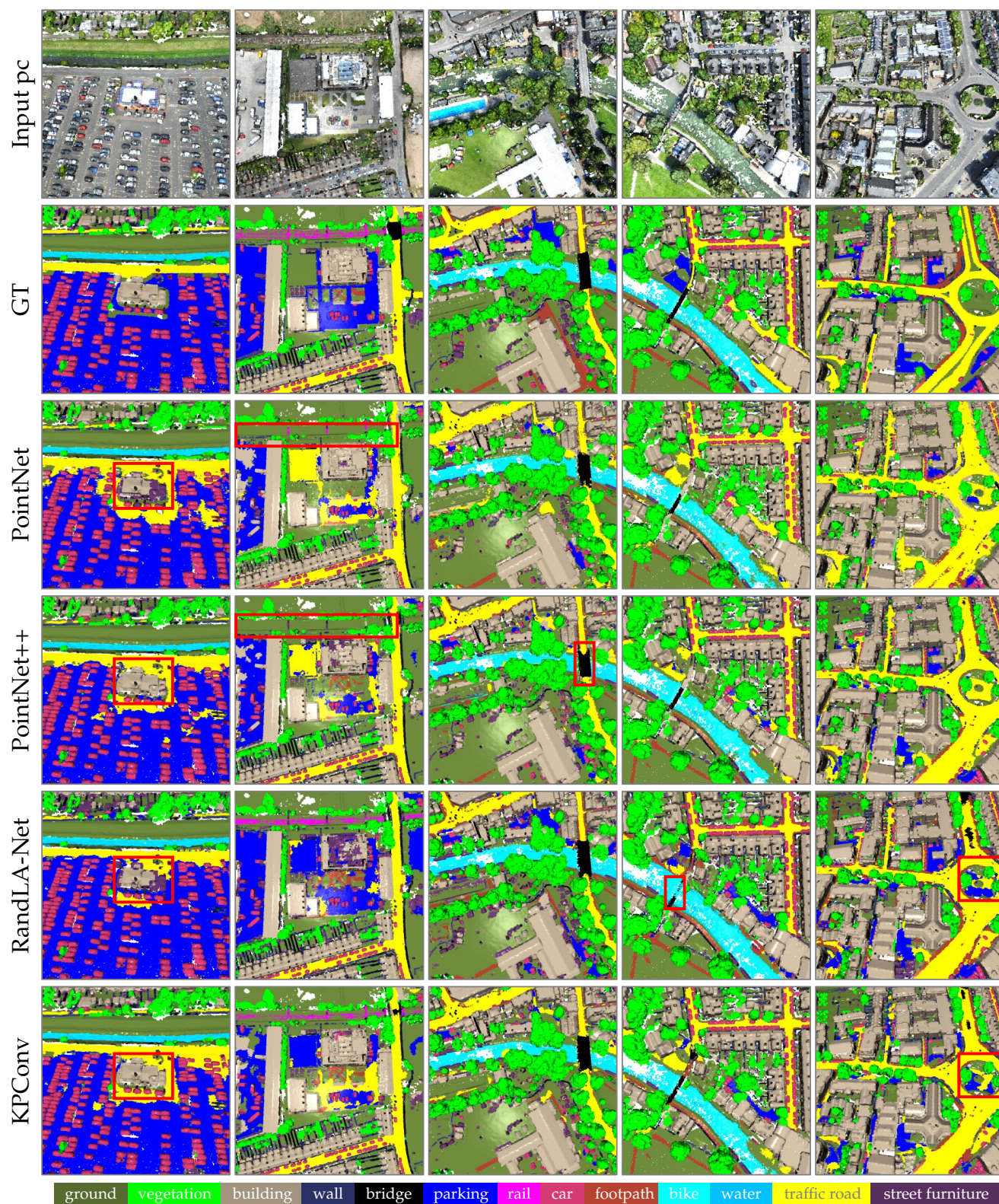


Fig. 7 Qualitative results of PointNet Qi et al. (2017a), PointNet++ Qi et al. (2017b), RandLA-Net Hu et al. (2020) and KPCConv Thomas et al. (2019) on the test set of SensatUrban dataset. The black dashed box highlights the inconsistency predictions with the ground-truth label.



## References

- Aksoy EE, Baci S, Cavdar S (2019) Salsanet: Fast road and vehicle segmentation in LiDAR point clouds for autonomous driving. In: 2020 IEEE Intelligent Vehicles Symposium (IV), pp 926–932
- Armeni I, Sax S, Zamir AR, Savarese S (2017) Joint 2D-3D-semantic data for indoor scene understanding. In: Proceedings of the IEEE/CVF International Conference on Computer Vision
- Behley J, Garbade M, Milioto A, Quenzel J, Behnke S, Stachniss C, Gall J (2019) SemanticKITTI: A dataset for semantic scene understanding of LiDAR sequences. In: Proceedings of the IEEE/CVF International Conference on Computer Vision, pp 9297–9307
- Berman M, Rannen Triki A, Blaschko MB (2018) The lovász-softmax loss: a tractable surrogate for the optimization of the intersection-over-union measure in neural networks. In: Proceedings of the IEEE/CVF International Conference on Computer Vision, pp 4413–4421
- Boulch A (2019) Generalizing discrete convolutions for unstructured point clouds. arXiv preprint arXiv:190402375
- Caesar H, Bankiti V, Lang AH, Vora S, Liong VE, Xu Q, Krishnan A, Pan Y, Baldan G, Beijbom O (2020) nuScenes: A multimodal dataset for autonomous driving. In: Proceedings of the IEEE/CVF International Conference on Computer Vision, pp 11621–11631
- Chang A, Dai A, Funkhouser T, Halber M, Niebner M, Savva M, Song S, Zeng A, Zhang Y (2018) Matterport3D: Learning from RGB-D data in indoor environments. In: 7th IEEE International Conference on 3D Vision, 3DV 2017, pp 667–676
- Chang AX, Funkhouser T, Guibas L, Hanrahan P, Huang Q, Li Z, Savarese S, Savva M, Song S, Su H, et al. (2015) ShapeNet: An information-rich 3D model repository. arXiv preprint arXiv:151203012
- Chang MF, Lambert J, Sangkloy P, Singh J, Bak S, Hartnett A, Wang D, Carr P, Lucey S, Ramanan D, et al. (2019) Argoverse: 3D tracking and forecasting with rich maps. In: Proceedings of the IEEE/CVF Conference on Computer Vision and Pattern Recognition, pp 8748–8757
- Chen T, Kornblith S, Norouzi M, Hinton G (2020) A simple framework for contrastive learning of visual representations. In: International Conference on Machine Learning, pp 1597–1607
- Cheng R, Razani R, Taghavi E, Li E, Liu B (2021) 2-s3net: Attentive feature fusion with adaptive feature selection for sparse semantic segmentation network. In: Proceedings of the IEEE/CVF Conference on Computer Vision and Pattern Recognition, pp 12547–12556
- Choy C, Gwak J, Savarese S (2019) 4D spatio-temporal convnets: Minkowski convolutional neural networks. In: Proceedings of the IEEE/CVF International Conference on Computer Vision, pp 3075–3084
- Cortinhal T, Tzelepis G, Aksoy EE (2020) Salsanext: Fast semantic segmentation of LiDAR point clouds for autonomous driving. arXiv preprint arXiv:200303653
- Dai A, Chang AX, Savva M, Halber M, Funkhouser T, Nießner M (2017) ScanNet: Richly-annotated 3D reconstructions of indoor scenes. In: Proceedings of the IEEE/CVF International Conference on Computer Vision, pp 5828–5839
- De Deuge M, Quadros A, Hung C, Douillard B (2013) Unsupervised feature learning for classification of outdoor 3D scans. In: Australasian Conference on Robotics and Automation, vol 2, p 1
- Gaidon A, Wang Q, Cabon Y, Vig E (2016) Virtual worlds as proxy for multi-object tracking analysis. In: Proceedings of the IEEE/CVF International Conference on Computer Vision, pp 4340–4349
- Geiger A, Lenz P, Urtasun R (2012) Are we ready for autonomous driving? the KITTI vision benchmark suite. In: 2012 IEEE Conference on Computer Vision and Pattern Recognition, pp 3354–3361
- Geiger A, Lenz P, Stiller C, Urtasun R (2013) Vision meets robotics: The kitti dataset. *The International Journal of Robotics Research* 32(11):1231–1237
- Gerke M, Kerle N (2011) Automatic structural seismic damage assessment with airborne oblique pictometry© imagery. *Photogrammetric Engineering & Remote Sensing* 77(9):885–898
- Geyer J, Kassahun Y, Mahmudi M, Ricou X, Durgesh R, Chung AS, Hauswald L, Pham VH, Mühlegg M, Dorn S, et al. (2020) A2D2: Audi autonomous driving dataset. arXiv preprint arXiv:200406320
- Graham B, Engelcke M, van der Maaten L (2018) 3D semantic segmentation with submanifold sparse convolutional networks. In: Proceedings of the IEEE/CVF International Conference on Computer Vision
- Guo Y, Wang H, Hu Q, Liu H, Liu L, Bennamoun M (2020) Deep learning for 3D point clouds: A survey. *IEEE TPAMI*
- Hackel T, Savinov N, Ladicky L, Wegner JD, Schindler K, Pollefeys M (2017) Semantic3D.Net: A new large-scale point cloud classification benchmark. *ISPRS Annals of Photogrammetry, Remote Sensing & Spatial Information Sciences*
- Han L, Zheng T, Xu L, Fang L (2020) Occuseg: Occupancy-aware 3d instance segmentation. In: Proceedings of the IEEE/CVF conference on computer vision and pattern recognition, pp 2940–2949
- Handa A, Patraucean V, Badrinarayanan V, Stent S, Cipolla R (2016) SceneNet: understanding real world indoor scenes with synthetic data. In: Proceedings of the IEEE/CVF International Conference on Computer Vision
- He K, Fan H, Wu Y, Xie S, Girshick R (2020) Momentum contrast for unsupervised visual representation learning. In:

- Proceedings of the IEEE/CVF Conference on Computer Vision and Pattern Recognition, pp 9729–9738
- Hou J, Graham B, Nießner M, Xie S (2020) Exploring data-efficient 3D scene understanding with contrastive scene contexts. arXiv preprint arXiv:201209165
- Hou L, Wang Y, Wang X, Maynard N, Cameron IT, Zhang S, Jiao Y (2014) Combining photogrammetry and augmented reality towards an integrated facility management system for the oil industry. *Proceedings of the IEEE* 102(2):204–220
- Hu J, You S, Neumann U (2003) Approaches to large-scale urban modeling. *IEEE Computer Graphics and Applications* 23(6):62–69
- Hu Q, Yang B, Xie L, Rosa S, Guo Y, Wang Z, Trigoni N, Markham A (2020) RandLA-Net: Efficient semantic segmentation of large-scale point clouds. In: *Proceedings of the IEEE/CVF International Conference on Computer Vision*
- Hu Q, Yang B, Khalid S, Xiao W, Trigoni N, Markham A (2021) Towards semantic segmentation of urban-scale 3d point clouds: A dataset, benchmarks and challenges. In: *Proceedings of the IEEE/CVF Conference on Computer Vision and Pattern Recognition*, pp 4977–4987
- Jiang L, Zhao H, Shi S, Liu S, Fu CW, Jia J (2020) Point-group: Dual-set point grouping for 3d instance segmentation. In: *Proceedings of the IEEE/CVF Conference on Computer Vision and Pattern Recognition*, pp 4867–4876
- Kölle M, Laupheimer D, Schmohl S, Haala N, Rottensteiner F, Wegner JD, Ledoux H (2021) H3d: Benchmark on semantic segmentation of high-resolution 3d point clouds and textured meshes from uav lidar and multi-view-stereo. arXiv preprint arXiv:210205346
- Landrieu L, Simonovsky M (2018) Large-scale point cloud semantic segmentation with superpoint graphs. In: *Proceedings of the IEEE/CVF International Conference on Computer Vision*, pp 4558–4567
- Lang AH, Vora S, Caesar H, Zhou L, Yang J, Beijbom O (2019) Pointpillars: Fast encoders for object detection from point clouds. In: *Proceedings of the IEEE/CVF Conference on Computer Vision and Pattern Recognition*, pp 12697–12705
- Le T, Duan Y (2018) PointGrid: A deep network for 3D shape understanding. In: *Proceedings of the IEEE/CVF International Conference on Computer Vision*, pp 9204–9214
- Lei H, Akhtar N, Mian A (2020) Spherical kernel for efficient graph convolution on 3D point clouds. *IEEE Transactions on Pattern Analysis and Machine Intelligence*
- Li X, Li C, Tong Z, Lim A, Yuan J, Wu Y, Tang J, Huang R (2020) Campus3D: A photogrammetry point cloud benchmark for hierarchical understanding of outdoor scene. *ACM MM*
- Li Y, Bu R, Sun M, Wu W, Di X, Chen B (2018) PointCNN: Convolution on X-transformed points. *Advances in Neural Information Processing Systems*
- Lin TY, Goyal P, Girshick R, He K, Dollár P (2017) Focal loss for dense object detection. *Proceedings of the IEEE/CVF International Conference on Computer Vision*
- Liu Z, Tang H, Lin Y, Han S (2019) Point-voxel cnn for efficient 3D deep learning. *Advances in Neural Information Processing Systems*
- Lyu Y, Huang X, Zhang Z (2020) Learning to segment 3D point clouds in 2D image space. In: *Proceedings of the IEEE/CVF International Conference on Computer Vision*
- McCormac J, Handa A, Leutenegger S, Davison AJ (2016) SceneNet RGB-D: 5m photorealistic images of synthetic indoor trajectories with ground truth. arXiv preprint arXiv:161205079
- Meng HY, Gao L, Lai YK, Manocha D (2019) VV-Net: Voxel vae net with group convolutions for point cloud segmentation. *Proceedings of the IEEE/CVF International Conference on Computer Vision*
- Milioto A, Vizzo I, Behley J, Stachniss C (2019) Rangenet++: Fast and accurate LiDAR semantic segmentation. In: 2019 *IEEE/RSJ International Conference on Intelligent Robots and Systems (IROS)*, pp 4213–4220
- Mo K, Zhu S, Chang AX, Yi L, Tripathi S, Guibas LJ, Su H (2019) PartNet: A large-scale benchmark for fine-grained and hierarchical part-level 3D object understanding. In: *Proceedings of the IEEE/CVF Conference on Computer Vision and Pattern Recognition*, pp 909–918
- Munoz D, Bagnell JA, Vandapel N, Hebert M (2009) Contextual classification with functional max-margin markov networks. In: *Proceedings of the IEEE/CVF International Conference on Computer Vision*
- Özdemir E, Toschi I, Remondino F (2019) a multi-purpose benchmark for photogrammetric urban 3D reconstruction in a controlled environment. In: *Evaluation and Benchmarking Sensors, Systems and Geospatial Data in Photogrammetry and Remote Sensing*, vol 42, pp 53–60
- Pan Y, Gao B, Mei J, Geng S, Li C, Zhao H (2020) Semantic-pose: A point cloud dataset with large quantity of dynamic instances. arXiv preprint arXiv:200209147
- Poursaeed O, Jiang T, Qiao Q, Xu N, Kim VG (2020) Self-supervised learning of point clouds via orientation estimation. arXiv preprint arXiv:200800305
- Qi CR, Su H, Mo K, Guibas LJ (2017a) PointNet: Deep learning on point sets for 3D classification and segmentation. In: *Proceedings of the IEEE/CVF International Conference on Computer Vision*, pp 652–660
- Qi CR, Yi L, Su H, Guibas LJ (2017b) PointNet++: Deep hierarchical feature learning on point sets in a metric space. *Advances in Neural Information Processing Systems*
- Qin N, Tan W, Ma L, Zhang D, Li J (2021) Opengf: An ultra-large-scale ground filtering dataset built upon open

- als point clouds around the world. In: Proceedings of the IEEE/CVF Conference on Computer Vision and Pattern Recognition, pp 1082–1091
- Rao D, Le QV, Phoka T, Quigley M, Sudsang A, Ng AY (2010) Grasping novel objects with depth segmentation. In: 2010 IEEE/RSJ International Conference on Intelligent Robots and Systems, pp 2578–2585
- Ros G, Sellart L, Materzynska J, Vazquez D, Lopez AM (2016) The SYNTHIA dataset: A large collection of synthetic images for semantic segmentation of urban scenes. In: Proceedings of the IEEE/CVF International Conference on Computer Vision, pp 3234–3243
- Rosu RA, Schütt P, Quenzel J, Behnke S (2019) LatticeNet: Fast point cloud segmentation using permutohedral lattices. arXiv preprint arXiv:191205905
- Rottensteiner F, Sohn G, Jung J, Gerke M, Baillard C, Benitez S, Breitkopf U (2012) The ISPRS benchmark on urban object classification and 3D building reconstruction. ISPRS Annals of the Photogrammetry, Remote Sensing and Spatial Information Sciences I-3 (2012), Nr 1 1(1):293–298
- Roynard X, Deschaud JE, Goulette F (2018) Paris-Lille-3D: A large and high-quality ground-truth urban point cloud dataset for automatic segmentation and classification. The International Journal of Robotics Research 37(6):545–557
- Sauder J, Sievers B (2019) Self-supervised deep learning on point clouds by reconstructing space. Advances in Neural Information Processing Systems pp 12962–12972
- Serna A, Marcotegui B, Goulette F, Deschaud JE (2014) Paris-rue-madame database: a 3D mobile laser scanner dataset for benchmarking urban detection, segmentation and classification methods. In: 4th International Conference on Pattern Recognition, Applications and Methods ICPRAM 2014
- Silberman N, Hoiem D, Kohli P, Fergus R (2012) Indoor segmentation and support inference from RGBD images. In: European conference on computer vision, pp 746–760
- Song S, Lichtenberg SP, Xiao J (2015) Sun RGB-D: A RGB-D scene understanding benchmark suite. In: Proceedings of the IEEE/CVF International Conference on Computer Vision, pp 567–576
- Sun P, Kretschmar H, Dotiwalla X, Chouard A, Patnaik V, Tsui P, Guo J, Zhou Y, Chai Y, Caine B, et al. (2020) Scalability in perception for autonomous driving: Waymo open dataset. In: Proceedings of the IEEE/CVF Conference on Computer Vision and Pattern Recognition, pp 2446–2454
- Tan W, Qin N, Ma L, Li Y, Du J, Cai G, Yang K, Li J (2020) Toronto-3D: A large-scale mobile LiDAR dataset for semantic segmentation of urban roadways. In: Proceedings of the IEEE/CVF Conference on Computer Vision and Pattern Recognition Workshops, pp 202–203
- Tang H, Liu Z, Zhao S, Lin Y, Lin J, Wang H, Han S (2020) Searching efficient 3D architectures with sparse point-voxel convolution. In: European Conference on Computer Vision, pp 685–702
- Tatarchenko M, Park J, Koltun V, Zhou QY (2018) Tangent convolutions for dense prediction in 3D. In: Proceedings of the IEEE/CVF International Conference on Computer Vision, pp 3887–3896
- Tchapmi L, Choy C, Armeni I, Gwak J, Savarese S (2017) Segcloud: Semantic segmentation of 3D point clouds. In: 2017 International Conference on 3D Vision (3DV), pp 537–547
- Thomas H, Qi CR, Deschaud JE, Marcotegui B, Goulette F, Guibas LJ (2019) KPConv: Flexible and deformable convolution for point clouds. Proceedings of the IEEE/CVF International Conference on Computer Vision pp 6411–6420
- Tong G, Li Y, Chen D, Sun Q, Cao W, Xiang G (2020) CSPC-dataset: New LiDAR point cloud dataset and benchmark for large-scale scene semantic segmentation. IEEE Access
- Uy MA, Pham QH, Hua BS, Nguyen T, Yeung SK (2019) Revisiting point cloud classification: A new benchmark dataset and classification model on real-world data. In: Proceedings of the IEEE/CVF International Conference on Computer Vision, pp 1588–1597
- Valada A, Vertens J, Dhall A, Burgard W (2017) Adapnet: Adaptive semantic segmentation in adverse environmental conditions. In: 2017 IEEE International Conference on Robotics and Automation (ICRA), pp 4644–4651
- Vallet B, Brédif M, Serna A, Marcotegui B, Paparoditis N (2015) TerraMobilita/iQmulus urban point cloud analysis benchmark. Computers & Graphics
- Varney N, Asari VK, Graehling Q (2020) DALES: A large-scale aerial LiDAR data set for semantic segmentation. In: Proceedings of the IEEE/CVF Conference on Computer Vision and Pattern Recognition Workshops, pp 186–187
- Wang H, Liu Q, Yue X, Lasenby J, Kusner MJ (2020) Pre-training by completing point clouds. arXiv preprint arXiv:201001089
- Wang L, Huang Y, Hou Y, Zhang S, Shan J (2019a) Graph attention convolution for point cloud semantic segmentation. In: Proceedings of the IEEE/CVF International Conference on Computer Vision
- Wang Y, Sun Y, Liu Z, Sarma SE, Bronstein MM, Solomon JM (2019b) Dynamic graph cnn for learning on point clouds. *Acm Transactions On Graphics (TOG)* 38(5):1–12
- Wei J, Lin G, Yap KH, Hung TY, Xie L (2020) Multi-path region mining for weakly supervised 3D semantic segmentation on point clouds. In: Proceedings of the IEEE/CVF Conference on Computer Vision and Pattern Recognition, pp 4384–4393
- Westoby MJ, Brasington J, Glasser NF, Hambrey MJ, Reynolds JM (2012) ‘structure-from-motion’ photogrammetry: A low-cost, effective tool for geoscience applications. *Geomorphology* 179:300–



314

- Wu B, Wan A, Yue X, Keutzer K (2018a) SqueezeSeg: Convolutional neural nets with recurrent CRF for real-time road-object segmentation from 3D LiDAR point cloud. In: 2018 IEEE International Conference on Robotics and Automation (ICRA), pp 1887–1893
- Wu B, Zhou X, Zhao S, Yue X, Keutzer K (2019) Squeeze-seg2: Improved model structure and unsupervised domain adaptation for road-object segmentation from a LiDAR point cloud. In: 2019 International Conference on Robotics and Automation (ICRA), pp 4376–4382
- Wu W, Qi Z, Fuxin L (2018b) PointConv: Deep convolutional networks on 3D point clouds. In: Proceedings of the IEEE/CVF International Conference on Computer Vision, pp 9621–9630
- Wu Z, Song S, Khosla A, Yu F, Zhang L, Tang X, Xiao J (2015) 3D ShapeNets: A deep representation for volumetric shapes. In: Proceedings of the IEEE/CVF International Conference on Computer Vision, pp 1912–1920
- Xie S, Gu J, Guo D, Qi CR, Guibas L, Litany O (2020) Point-contrast: Unsupervised pre-training for 3D point cloud understanding. In: European Conference on Computer Vision, pp 574–591
- Xu C, Wu B, Wang Z, Zhan W, Vajda P, Keutzer K, Tomizuka M (2020) SqueezeSegV3: Spatially-adaptive convolution for efficient point-cloud segmentation. In: Proceedings of the European Conference on Computer Vision (ECCV), pp 1–19
- Xu X, Lee GH (2020) Weakly supervised semantic point cloud segmentation: Towards 10x fewer labels. In: Proceedings of the IEEE/CVF Conference on Computer Vision and Pattern Recognition, pp 13706–13715
- Yan X, Zheng C, Li Z, Wang S, Cui S (2020) PointASNL: Robust point clouds processing using nonlocal neural networks with adaptive sampling. In: Proceedings of the IEEE/CVF International Conference on Computer Vision, pp 5589–5598
- Yang B, Wang J, Clark R, Hu Q, Wang S, Markham A, Trigoni N (2019) Learning object bounding boxes for 3D instance segmentation on point clouds. *Advances in Neural Information Processing Systems*
- Ye X, Li J, Huang H, Du L, Zhang X (2018) 3D recurrent neural networks with context fusion for point cloud semantic segmentation. In: Proceedings of the European Conference on Computer Vision (ECCV)
- Ye Z, Xu Y, Huang R, Tong X, Li X, Liu X, Luan K, Hoegner L, Stilla U (2020) LASDU: A large-scale aerial LiDAR dataset for semantic labeling in dense urban areas. *ISPRS International Journal of Geo-Information* 9(7):450
- Yi L, Kim VG, Ceylan D, Shen IC, Yan M, Su H, Lu C, Huang Q, Sheffer A, Guibas L (2016) A scalable active framework for region annotation in 3D shape collections. *ACM Transactions on Graphics (TOG)* 35(6):1–12
- Yuan W, Khot T, Held D, Mertz C, Hebert M (2018) PCN: Point completion network. In: 2018 International Conference on 3D Vision (3DV), pp 728–737
- Zhang Y, Zhou Z, David P, Yue X, Xi Z, Gong B, Foroosh H (2020) PolarNet: An improved grid representation for online LiDAR point clouds semantic segmentation. In: Proceedings of the IEEE/CVF International Conference on Computer Vision, pp 9601–9610
- Zhang Z, Gerke M, Vosselman G, Yang MY (2018) A patch-based method for the evaluation of dense image matching quality. *International journal of applied earth observation and geoinformation* 70:25–34
- Zhang Z, Hua BS, Yeung SK (2019) ShellNet: Efficient point cloud convolutional neural networks using concentric shells statistics. Proceedings of the IEEE/CVF International Conference on Computer Vision pp 1607–1616
- Zhang Z, Girdhar R, Joulin A, Misra I (2021) Self-supervised pretraining of 3D features on any point-cloud. arXiv preprint arXiv:210102691
- Zhao H, Jiang L, Jia J, Torr P, Koltun V (2020) Point transformer. arXiv preprint arXiv:201209164
- Zhou B, Zhao H, Puig X, Fidler S, Barriuso A, Torralba A (2017) Scene parsing through ADE20K dataset. In: Proceedings of the IEEE/CVF International Conference on Computer Vision, pp 633–641
- Zhou Y, Tuzel O (2018) VoxelNet: End-to-end learning for point cloud based 3D object detection. In: Proceedings of the IEEE/CVF International Conference on Computer Vision, pp 4490–4499
- Zhu X, Zhou H, Wang T, Hong F, Ma Y, Li W, Li H, Lin D (2021) Cylindrical and asymmetrical 3D convolution networks for LiDAR segmentation. In: Proceedings of the IEEE/CVF Conference on Computer Vision and Pattern Recognition
- Zolanvari S, Ruano S, Rana A, Cummins A, da Silva RE, Rahbar M, Smolic A (2019) DublinCity: Annotated LiDAR point cloud and its applications. In: British Machine Vision Conference